J. Fluid Mech. (2012), *vol.* 711, *pp.* 337–363.
doi:10.1017/jfm.2012.395

Oblique collisions of internal wave beams and associated resonances

T. R. Akylas† and H. H. Karimi

Department of Mechanical Engineering, Massachusetts Institute of Technology, Cambridge, MA 02139, USA

(Received 12 January 2012; revised 28 May 2012; accepted 2 August 2012; first published online 19 September 2012)

Quadratic nonlinear interactions between two colliding internal gravity wave beams in a uniformly stratified fluid, and the resulting radiation of secondary beams with frequencies equal to the sum and difference of those of the primary beams, are discussed. The analysis centres on oblique collisions, involving beams that propagate in different vertical planes. The propagation directions of generated secondary beams are deduced from kinematic considerations and the use of radiation conditions, thus extending to oblique collisions previously derived selection rules for plane collisions. Using small-amplitude expansions, radiated-beam profiles at steady state are also computed in terms of the characteristics of the colliding beams. It is pointed out that, for certain oblique collision configurations, radiated beams with frequency equal to the difference of the primary frequencies have unbounded steady-state amplitude. This resonance, which has no counterpart for plane collisions, is further analysed via the solution of an initial-value problem; ignoring dissipation, the transient resonant response grows in time like $t^{1/2}$, a behaviour akin to that of forced waves at cut-off frequencies.

Key words: internal waves, ocean processes, stratified flows

1. Introduction

Internal gravity wave beams are time-harmonic plane-wave disturbances with a general spatial profile in continuously stratified fluids. According to the dispersion relation of this anisotropic wave motion, the frequency of a sinusoidal plane wave depends solely on the orientation of the wavevector relative to the vertical, and energy is transported along, rather than perpendicularly, to the wave crests. As a result, a two-dimensional, spatially localized time-harmonic source, instead of cylindrical wavefronts, gives rise to an X-shape pattern comprising four wave beams that stretch radially outwards from the source (see, for example, Lighthill 1978, § 4.4). This rather unusual wave pattern, known as 'St Andrew's Cross', was generated in the laboratory by Mowbray & Rarity (1967) using as source an oscillating cylinder in a stratified fluid tank, thereby also producing the first experimental documentation of internal wave beams.

More recent studies of internal wave beams are motivated mostly by ocean-related problems. In this context, a matter of considerable interest is the interaction of the barotropic tide with sea-floor topographic features and the associated transfer of energy

† Email address for correspondence: trakylas@MIT.EDU

to internal waves, a process that is believed to be important in deep-ocean mixing. The role of internal wave beams in this so-called tidal conversion was brought out by Bell (1975). Based on the linearized governing equations, he studied the generation of internal waves by a time-harmonic current of uniformly stratified fluid of infinite depth, representing the tide, over locally confined topography of small steepness. The far-field response according to this simple model comprises radiating wave beams at the tidal frequency and its harmonics below the buoyancy frequency of the background flow. Later, Khatiwala (2003) accounted for the effects of a finite ocean in Bell's model, and Lamb (2004) carried out fully numerical simulations of tidal flow over a ridge of finite steepness. The latter study first directed attention to the significance of nonlinear interactions between internal wave beams. Such interactions may occur close to boundaries where an incident and reflected beam meet, and give rise to additional reflected beams with frequencies equal to the harmonics of that of the incident beam. In addition, nonlinear interactions are possible in the interior of the flow where two wave beams of different frequencies may collide, resulting in the radiation of new beams with frequencies equal to the sum and difference of those of the colliding beams. These nonlinear mechanisms are also evident in later numerical simulations (Gerkema, Staquet & Bouruet-Aubertot 2006) as well as in laboratory experiments (Peacock & Tabaei 2005; Zhang, King & Swinney 2007) and field observations (Stashchuk & Vlasenko 2005).

In the further development of the theory, Tabaei, Akylas & Lamb (2005) studied nonlinear interactions of wave beams in a stationary uniformly stratified fluid. Using small-amplitude expansions, they computed steady-state profiles of radiated secondary beams resulting from reflections at a sloping boundary and from collisions of two freely propagating beams. An essential element in this steady-state analysis is the use of suitable radiation conditions, to ensure that the primary and the emitted secondary beams transport energy in accordance with causality. As a result of these conditions, not all secondary beams that are geometrically admissible may be excited by quadratic interactions. For beam collisions, in particular, Jiang & Marcus (2009), by examining in detail the restrictions imposed by radiation conditions, derived a set of rules for predicting which secondary beams, of the eight in total that are possible geometrically in each collision configuration, can in fact be generated by quadratic interactions. We remark that some of these restrictions were overlooked in table 1 and in figures 6 and 7 of Tabaei *et al.* (2005). However, (5.9) and (5.14) in Tabaei *et al.* (2005), which provide explicit expressions for the radiated-beam profiles, observe the appropriate radiation conditions and are consistent with the selection rules of Jiang & Marcus (2009).

In contrast to the studies cited above, which assume two-dimensional flow and hence planar interactions of internal wave beams, the present paper is concerned with three-dimensional interactions due to collisions of beams that propagate in different vertical planes. As revealed by recent laboratory experiments and direct numerical simulations, oscillatory flow over a three-dimensional bottom obstacle can generate second-harmonic wave beams not only along, but also perpendicularly to the flow direction (King, Zhang & Swinney 2010). This suggests that oblique beam collisions of the type discussed here may arise from the interaction of the tide with complex three-dimensional topography.

In oblique collisions, quadratic interactions again give rise to new beams with frequencies equal to the sum and difference of those of the colliding beams, but the propagation directions of the radiated beams are not obvious. Using kinematic arguments and suitable radiation conditions, we first determine the propagation

direction of each emitted secondary beam, thus extending to oblique collisions the selection rules derived in Jiang & Marcus (2009) for plane collisions. Attention is then focused on computing steady-state profiles of secondary beams, employing small-amplitude expansions along the lines of Tabaei *et al.* (2005). Sample computations suggest that, as the degree of obliqueness of a collision is varied, radiated beams with frequency equal to the sum of the frequencies of the colliding beams are strongest for a plane collision. On the other hand, it turns out that radiated beams with frequency equal to the difference of the primary frequencies have unbounded steady-state amplitude for certain oblique orientations of the colliding beams. This interesting feature of oblique collisions is further analysed by solving an initial-value problem that mimics the gradual development of secondary beams, following the collision of the two primary beams. At the critical conditions where the steady-state beam amplitude is unbounded, ignoring dissipation, the transient response grows in time like $t^{1/2}$, a resonance similar to that found for forced waves at cut-off frequencies in simpler problems (Aranha, Yue & Mei 1982; Akylas 1984). Resonant collisions of internal wave beams may thus prove to be an efficient mechanism for significant energy exchange between colliding and radiated beams.

The present analysis can be readily extended to include the effects of background rotation, which may influence collisions of tidally generated wave beams.

2. Preliminaries

Employing the same scalings as in Tabaei & Akylas (2003), the equations governing inviscid, incompressible, uniformly stratified Boussinesq flow take the dimensionless form

$$\boldsymbol{\nabla}\cdot\boldsymbol{u}=0, \tag{2.1}$$

$$\rho_t+\boldsymbol{u}\cdot\boldsymbol{\nabla}\rho-w=0, \tag{2.2}$$

$$\boldsymbol{u}_t+\boldsymbol{u}\cdot\boldsymbol{\nabla}\boldsymbol{u}=-\boldsymbol{\nabla}p-\rho\boldsymbol{e}_z. \tag{2.3}$$

Here, $\boldsymbol{u}=(u,v,w)$ is the velocity field, p and ρ are the reduced pressure and density, respectively, and $\boldsymbol{e}_z$ is a unit vector pointing upwards along the vertical (z) direction. Under the assumed flow conditions, the Brunt–Väisälä frequency is constant and has been normalized to unity.

From the equation system (2.1)–(2.3), by straightforward manipulation, it follows that

$$\nabla^2 w_{tt}+\nabla_H^2 w=\mathscr{R}, \tag{2.4}$$

where

$$\mathscr{R}=\nabla_H^2\{\boldsymbol{u}\cdot\boldsymbol{\nabla}\rho-(\boldsymbol{u}\cdot\boldsymbol{\nabla}w)_t\}+\{\boldsymbol{\nabla}_H\cdot(\boldsymbol{u}\cdot\boldsymbol{\nabla}\boldsymbol{u}_H)\}_{zt}, \tag{2.5}$$

$\boldsymbol{u}_H=(u,v)$ being the velocity, $\boldsymbol{\nabla}_H=(\partial/\partial x,\partial/\partial y)$ the gradient and $\nabla_H^2=\partial^2/\partial x^2+\partial^2/\partial y^2$ the Laplacian in the horizontal plane. Note that the linear part of (2.4) involves only the vertical velocity w, and the nonlinear terms have been grouped together on the right-hand side. This equation will prove particularly useful in the ensuing analysis.

The left-hand side of (2.4) confirms that the frequency ω of sinusoidal plane waves obeys the well-known dispersion relation of internal gravity waves,

$$\omega^2=\sin^2\theta, \tag{2.6}$$

where θ denotes the angle of inclination to the vertical of the wavevector $\boldsymbol{k} = k(\sin\theta\cos\phi,\ \sin\theta\sin\phi, \cos\theta)$. Since ω is independent of the wavevector magnitude k and the azimuthal angle ϕ, the group velocity $\boldsymbol{c}_g = \boldsymbol{\nabla}_k\omega$ is orthogonal to the phase velocity $\boldsymbol{c} = (\omega/k^2)\boldsymbol{k}$ and $\boldsymbol{c}_g$ lies in the same vertical plane as $\boldsymbol{c}$. Moreover, as it turns out, $\boldsymbol{c}$ and $\boldsymbol{c}_g$ have opposite vertical components:

$$\boldsymbol{c}_g \cdot \boldsymbol{c} = 0, \tag{2.7a}$$

$$(\boldsymbol{c} + \boldsymbol{c}_g) \cdot \boldsymbol{e}_z = 0. \tag{2.7b}$$

The fact that ω is independent of k makes it possible to construct plane wave beams, by superposing sinusoidal plane waves with wavevectors $\boldsymbol{k}$ pointing along a fixed direction:

$$\boldsymbol{u} = \boldsymbol{U}(\eta)\mathrm{e}^{-\mathrm{i}\omega t} + \text{c.c.}, \quad \rho = R(\eta)\mathrm{e}^{-\mathrm{i}\omega t} + \text{c.c.}, \tag{2.8}$$

where c.c. denotes the complex conjugate and

$$\boldsymbol{U} = \int_0^\infty \hat{\boldsymbol{U}}(k)\mathrm{e}^{\mathrm{i}k\eta}\,\mathrm{d}k, \quad R = \int_0^\infty \hat{R}(k)\mathrm{e}^{\mathrm{i}k\eta}\,\mathrm{d}k, \tag{2.9}$$

with

$$\hat{\boldsymbol{U}} = A(k)(-\cot\theta\cos\phi, -\cot\theta\sin\phi, 1), \tag{2.10a}$$

$$\hat{R} = \frac{\mathrm{i}}{\sin\theta}A(k). \tag{2.10b}$$

This class of wave disturbances is uniform in the along-beam direction, which coincides with $\boldsymbol{c}_g$, and the velocity and density profiles (2.9) are functions of the cross-beam coordinate $\eta = x\sin\theta\cos\phi + y\sin\theta\sin\phi + z\cos\theta$ alone. Also, in view of (2.1), $\boldsymbol{u}$ is perpendicular to $\boldsymbol{k}$ and hence to the cross-beam direction as well; as a result, the nonlinear terms in (2.2)–(2.3) and (2.4) vanish, and uniform wave beams of the form (2.8) are exact nonlinear solutions irrespective of the spectral amplitude $A(k)$ in (2.10) (McEwan 1973; Tabaei & Akylas 2003).

The choice of the range of integration over k in (2.9) is in keeping with uni-directional transport of energy. For each sinusoidal plane wave partaking in a beam, the direction of energy propagation is along the group velocity $\boldsymbol{c}_g$, which obeys conditions (2.7); letting $\boldsymbol{k} \to -\boldsymbol{k}$, in particular, $\boldsymbol{c}_g \to -\boldsymbol{c}_g$. Therefore, fixing the sign of ω, uni-directional beams, which transport energy in one direction, involve sinusoidal plane waves with wavenumbers of the same sign only.

Although an isolated uniform beam is a nonlinear solution, this is no longer true for the superposition of non-collinear beams because of nonlinear interactions that come into play in the region where these beams overlap. The present study focuses on the effects of quadratic nonlinear interactions between two colliding wave beams of small amplitude, in the three-dimensional configuration where the beam propagation directions lie in different vertical planes; collisions of this type will be referred to as oblique.

3. Kinematics

Consider two uni-directional plane wave beams approaching each other at angles θ_1 and θ_2 $(0 < \theta_1, \theta_2 < \pi/2)$ to the horizontal, their corresponding frequencies being $\omega_1 = \sin\theta_1 > 0$ and $\omega_2 = \sin\theta_2 > 0$, according to (2.6). As our interest centres on oblique collisions, the propagation directions of the two beams (specified by the directions of the group velocities $\boldsymbol{c}_{g_1}$ and $\boldsymbol{c}_{g_2}$) are taken to be in different vertical

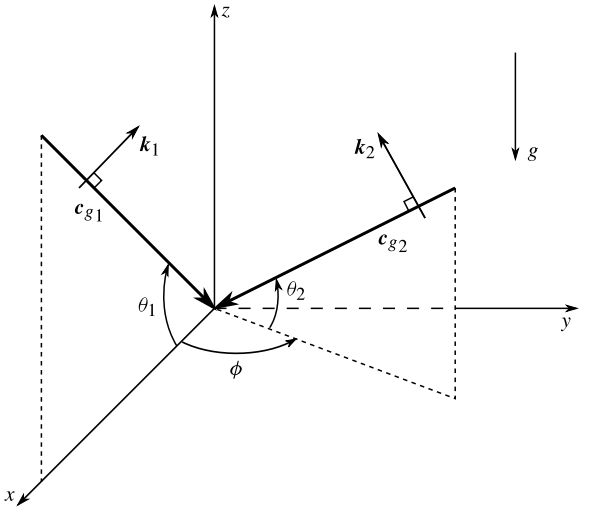

FIGURE 1. Geometry of collision of two uniform wave beams approaching each other at angles θ_1 and θ_2 to the horizontal. The colliding beams have propagation directions (specified by the corresponding group velocities $\boldsymbol{c}_{g1}$ and $\boldsymbol{c}_{g2}$) that lie in different vertical planes. The azimuthal angle ϕ controls the obliqueness of the collision, with $\phi = 0, \pi$ corresponding to plane collisions in the xz-plane. The beam of frequency $\omega_1 = \sin\theta_1 > 0$ is taken to propagate downwards in z while the beam of frequency $0 < \omega_2 = \sin\theta_2 < \omega_1$ propagates downwards (as shown here) or upwards in z.

planes, and the azimuthal angle ϕ controls the degree of obliqueness of the collision (figure 1).

More specifically, the two colliding beams comprise sinusoidal plane waves with frequencies ω_1 and ω_2 and wavevectors

$$\boldsymbol{k}_1 = k_1(-\sin\theta_1, 0, \cos\theta_1) \quad (k_1 > 0), \tag{3.1a}$$

$$\boldsymbol{k}_2 = k_2(-\sin\theta_2\cos\phi, -\sin\theta_2\sin\phi, \pm\cos\theta_2) \quad (k_2 > 0). \tag{3.1b}$$

Recalling conditions (2.7) obeyed by the group and phase velocities, the wavevectors in (3.1) are such that the beam of frequency ω_1 propagates downwards in z while the beam of frequency ω_2 propagates downwards or upwards in z when the vertical wavevector component in (3.1*b*) is positive (upper sign) or negative (lower sign), respectively. Also, without any loss, the angle ϕ is taken in the range

$$0 \leqslant \phi \leqslant \pi, \tag{3.2}$$

with $\phi = 0$ and $\phi = \pi$ corresponding to plane collisions in the xz-plane. Finally, it is assumed throughout that $\theta_1 > \theta_2$ and hence $\omega_1 > \omega_2$. (Details for other collision configurations can be worked out along similar lines.)

In the region where the two uniform beams overlap, quadratic nonlinear interactions generate the sum and difference of the colliding-beam frequencies,

$$\omega^+ = \omega_1 + \omega_2, \quad \omega^- = \omega_1 - \omega_2, \tag{3.3}$$

along with sums and differences of the wavevectors (3.1):

$$\boldsymbol{k}^+ = \boldsymbol{k}_1 + \boldsymbol{k}_2, \quad \boldsymbol{k}^- = \boldsymbol{k}_1 - \boldsymbol{k}_2. \tag{3.4}$$

We now inquire whether, on kinematic grounds, these frequencies and corresponding wavevectors are compatible with disturbances radiating in the far field, away from the interaction region of the colliding beams.

3.1. *Beams with frequency* ω^+

According to (2.6), for disturbances with frequency ω^+ to radiate, it is necessary that $\omega^+ < 1$. Assuming this to be the case, we write

$$\omega^+ = \sin\theta_1 + \sin\theta_2 = \sin\theta^+ \quad (0 < \theta^+ < \pi/2), \tag{3.5}$$

where θ^+ is the propagation angle to the horizontal of internal waves of frequency ω^+.

Turning to the associated wavevectors $\boldsymbol{k}^+$, it follows from (3.1) and (3.4) that

$$\boldsymbol{k}^+ = (-k_1\sin\theta_1 - k_2\sin\theta_2\cos\phi,\, -k_2\sin\theta_2\sin\phi,\, k_1\cos\theta_1 \pm k_2\cos\theta_2) \tag{3.6}$$

with $k_1 > 0$ and $k_2 > 0$. It is convenient to express this set of wavevectors in the form

$$\boldsymbol{k}^+ = \kappa(\sin\theta^+\cos\psi,\, \sin\theta^+\sin\psi,\, m) \quad (\kappa > 0), \tag{3.7}$$

where, from (3.6),

$$m = \frac{\sin\theta^+}{\sin\phi}(\cot\theta_1\sin(\psi - \phi) \mp \cot\theta_2\sin\psi) \tag{3.8}$$

and

$$k_1 = \kappa\frac{\sin\theta^+\sin(\psi - \phi)}{\sin\phi\sin\theta_1}, \quad k_2 = -\kappa\frac{\sin\theta^+\sin\psi}{\sin\phi\sin\theta_2}. \tag{3.9}$$

Given that $\sin\phi \gtrless 0$ in view of (3.2) and $\kappa > 0$, the conditions $k_1 > 0$ and $k_2 > 0$ require

$$\pi < \psi < \pi + \phi. \tag{3.10}$$

Among the waves with frequency ω^+ and wavevector $\boldsymbol{k}^+$ in the form (3.7), those that can propagate in the far field must also be compatible with the internal-wave dispersion relation (2.6). This implies

$$m^2 = \cos^2\theta^+. \tag{3.11}$$

Moreover, causality requires that radiating waves transport energy away from the wave source. Hence, the vertical component of the group velocity must be positive for waves radiating in $z > 0$ and negative for waves radiating in $z < 0$. Making use of (2.7*b*), this radiation condition then specifies the sign of the vertical component of $\boldsymbol{k}^+$:

$$m = \mp\cos\theta^+ \quad (z \gtrless 0). \tag{3.12}$$

For waves propagating in $z > 0$, in particular, combining (3.8) with (3.12) yields

$$F^+_\mp(\psi) \equiv \cot\theta_1\sin(\psi - \phi) \mp \cot\theta_2\sin\psi + \sin\phi\cot\theta^+ = 0, \tag{3.13}$$

where, in line with (3.1*b*), the upper (lower) sign applies when the beam with frequency ω_2 propagates downwards (upwards) in z. For given ω_1 and ω_2, the angles θ_1, θ_2 and θ^+ are fixed, and (3.13) determines ψ as a function of the angle $0 < \phi < \pi$ that controls the obliqueness of the collision. Thus, upon varying $\kappa > 0$ in (3.7), each root ψ of (3.13) in the range (3.10) furnishes a uniform beam that radiates in $z > 0$, with the angle ψ measuring the obliqueness of this beam relative to the xz-plane.

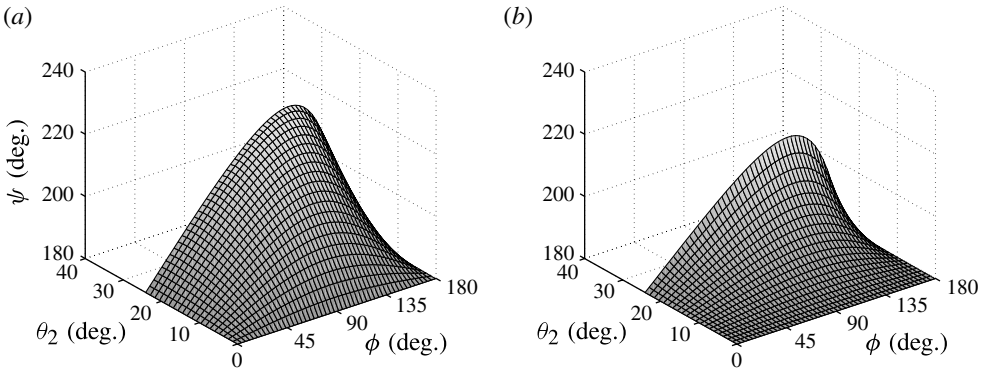

FIGURE 2. Obliqueness angle ψ of induced secondary beam with frequency ω^+, as a function of the angle $0° < \phi < 180°$ that controls the obliqueness of the collision (see figure 1): (*a*) beam radiating in $z > 0$; (*b*) beam radiating in $z < 0$. The colliding beams propagate at angles $\theta_1 = 35°$ and $0° < \theta_2 < 24.41°$ such that $\omega^+ < 1$.

Save for the special cases $\phi = 0,\ \pi$ corresponding to plane collisions, ψ is found by solving numerically (3.13) subject to (3.10). When both colliding beams propagate downwards in z, as $\sin\phi > 0$, $\sin\psi < 0$ and $\sin(\psi - \phi) > 0$, there are no acceptable solutions of $F^+_-(\psi) = 0$, so no secondary beams with frequency ω^+ that radiate in $z > 0$ are possible. On the other hand, when the beam with frequency ω_2 propagates upwards, there is one acceptable root of $F^+_+(\psi) = 0$, and hence one secondary beam radiating in $z > 0$, for each $0 < \phi < \pi$. Computed values of ψ as a function of ϕ for $\theta_1 = 35°$ and θ_2 in the range $0 < \theta_2 < 24.41°$, where $\omega^+ < 1$, are plotted in figure 2(*a*).

The possibility of secondary beams with frequency ω^+ radiating in $z < 0$ can be examined in a similar way. In this instance, from (3.8) and (3.12), one obtains the following equation for ψ:

$$G^+_\mp(\psi) \equiv \cot\theta_1 \sin(\psi - \phi) \mp \cot\theta_2 \sin\psi - \sin\phi \cot\theta^+ = 0, \tag{3.14}$$

where again the upper (lower) sign applies when the beam with frequency ω_2 propagates downwards (upwards) in z. Qualitatively, the results are similar to those found above for secondary beams radiating in $z > 0$: no secondary beam is possible when both colliding beams propagate downwards in z and one such beam is generated for each $0 < \phi < \pi$ when the beam of frequency ω_2 propagates upwards in z. Computed values of ψ as a function of ϕ are plotted in figure 2(*b*) for $\theta_1 = 35°$ and θ_2 in the range $0 < \theta_2 < 24.41°$, where $\omega^+ < 1$.

The results obtained here for obliquely colliding beams may be viewed as generalizations of the selection rules derived by Jiang & Marcus (2009) for plane collisions ($\phi = 0, \pi$) of two beams. These rules can be readily deduced from (3.8), (3.9) and (3.12) in conjunction with the conditions $k_1 > 0$ and $k_2 > 0$. Specifically, in the case of secondary beams radiating in $z > 0$, it follows from (3.8) and (3.12) that

$$\frac{\sin\psi}{\sin\phi} = \frac{\cos\psi\cot\theta_1 - \cot\theta^+}{\cot\theta_1\cos\phi \mp \cot\theta_2}, \tag{3.15a}$$

$$\frac{\sin(\psi - \phi)}{\sin\phi} = \frac{-\cot\theta^+\cos\phi \pm \cot\theta_2\cos\psi}{\cot\theta_1\cos\phi \mp \cot\theta_2}. \tag{3.15b}$$

In view of (3.9), $k_1 > 0$ and $k_2 > 0$ then require

$$\frac{\cos\psi\cot\theta_1 - \cot\theta^+}{\cot\theta_1\cos\phi \mp \cot\theta_2} < 0, \tag{3.16a}$$

$$\frac{-\cot\theta^+\cos\phi \pm \cot\theta_2\cos\psi}{\cot\theta_1\cos\phi \mp \cot\theta_2} > 0. \tag{3.16b}$$

In a similar way, for secondary beams radiating in $z < 0$, making use of (3.8), (3.9) and (3.12), one finds that the conditions $k_1 > 0$ and $k_2 > 0$ translate to

$$\frac{\cos\psi\cot\theta_1 + \cot\theta^+}{\cot\theta_1\cos\phi \mp \cot\theta_2} < 0, \tag{3.17a}$$

$$\frac{\cot\theta^+\cos\phi \pm \cot\theta_2\cos\psi}{\cot\theta_1\cos\phi \mp \cot\theta_2} > 0. \tag{3.17b}$$

In both (3.16) and (3.17), the upper (lower) sign holds when the beam of frequency ω_2 propagates downwards (upwards) in z.

It is now straightforward to check on a case-by-case basis whether conditions (3.16) and (3.17) can be met for plane collisions in the xz-plane, by taking $\phi = 0$ (the beam with frequency ω_2 is incident from the first or fourth quadrant) or $\phi = \pi$ (this beam is incident from the second or third quadrant) and $\psi = 0$ (a secondary beam is radiated in the first or fourth quadrant) or $\psi = \pi$ (a secondary beam is radiated in the second or third quadrant). In agreement with Jiang & Marcus (2009), for $\theta_1 > \theta_2$, we find that secondary beams can be found in the second and third quadrants ($\psi = \pi$) only; they arise when the beam of frequency ω_2 propagates upwards in z and is incident from either the third ($\phi = \pi$) or fourth ($\phi = 0$) quadrant.

3.2. *Beams with frequency* ω^-

Since $0 < \omega^- = \omega_1 - \omega_2 < 1$, internal waves with frequency ω^- can always propagate at an angle θ^- to the horizontal fixed by the dispersion relation (2.6):

$$\omega^- = \sin\theta_1 - \sin\theta_2 = \sin\theta^- \quad (0 < \theta^- < \pi/2). \tag{3.18}$$

Moreover, from (3.1) and (3.4), the associated set of wavevectors $\boldsymbol{k}^-$ is

$$\boldsymbol{k}^- = (-k_1\sin\theta_1 + k_2\sin\theta_2\cos\phi, k_2\sin\theta_2\sin\phi, k_1\cos\theta_1 \mp k_2\cos\theta_2) \tag{3.19}$$

with $k_1 > 0$ and $k_2 > 0$.

As in the analysis of beams with frequency ω^+ earlier, we now write

$$\boldsymbol{k}^- = \kappa(\sin\theta^-\cos\psi, \sin\theta^-\sin\psi, m) \quad (\kappa > 0), \tag{3.20}$$

where, from (3.19),

$$m = \frac{\sin\theta^-}{\sin\phi}(\cot\theta_1\sin(\psi - \phi) \mp \cot\theta_2\sin\psi), \tag{3.21}$$

and

$$k_1 = \kappa\frac{\sin\theta^-\sin(\psi - \phi)}{\sin\phi\sin\theta_1}, \quad k_2 = \kappa\frac{\sin\theta^-\sin\psi}{\sin\phi\sin\theta_2}. \tag{3.22}$$

Given that $0 \leqslant \phi \leqslant \pi$ and $\kappa > 0$, it follows from (3.22) that the conditions $k_1 > 0$ and $k_2 > 0$ here confine ψ in the range

$$\phi < \psi < \pi. \tag{3.23}$$

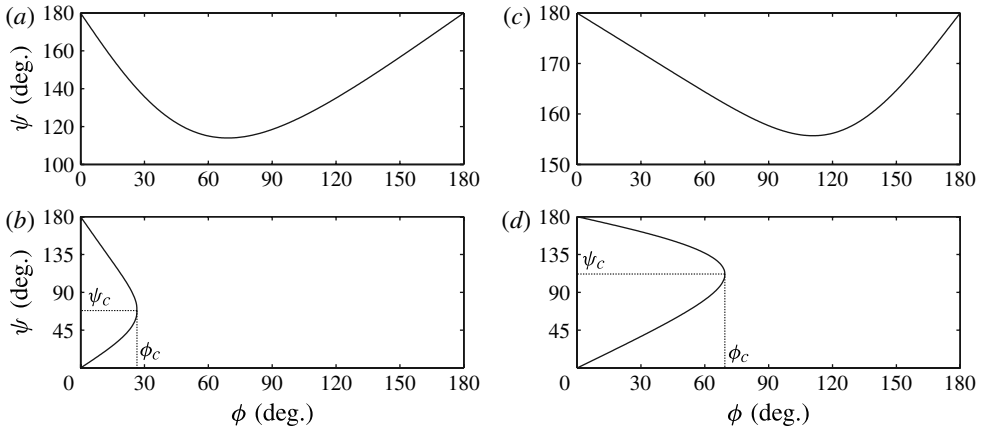

FIGURE 3. Obliqueness angle ψ of induced secondary beams with frequency ω^-, as a function of the angle $0° < \phi < 180°$ that controls the obliqueness of the collision (figure 1): (*a*,*b*) beams radiating in $z > 0$; (*c*,*d*) beams radiating in $z < 0$. The colliding beams propagate at angles $\theta_1 = 35°$ and $\theta_2 < \theta_1$: (*a*,*c*) $\theta_2 = 14°$ $(\omega_2/\omega_1 = 0.422)$; (*b*,*d*) $\theta_2 = 19°$ $(\omega_2/\omega_1 = 0.568)$. The critical $\phi = \phi_c$ and the corresponding $\psi = \psi_c$ are marked in (*b*,*d*).

The next step is to ensure that the wavevectors $\boldsymbol{k}^-$ in (3.20) and the frequency $\omega^- = \sin\theta^-$ satisfy the dispersion relation (2.6). In addition, causality requires that radiating waves transport energy to the far field; thus, the vertical component of the group velocity must be positive for waves that are found in $z > 0$ and negative for waves that are found in $z < 0$. Imposing these conditions specifies m in (3.20):

$$m = \mp \cos\theta^- \quad (z \gtrless 0). \tag{3.24}$$

Now, for waves found in $z > 0$, combining (3.24) with (3.21) yields

$$F^-_{\mp}(\psi) \equiv \cot\theta_1 \sin(\psi - \phi) \mp \cot\theta_2 \sin\psi + \sin\phi \cot\theta^- = 0, \tag{3.25}$$

the upper (lower) sign being valid when the beam of frequency ω_2 propagates downwards (upwards) in z. For each $0 < \phi < \pi$, this equation subject to the constraint (3.23) determines ψ, which, in view of (3.20), measures the obliqueness relative to the xz-plane of the induced beam in $z > 0$.

In general, (3.25) is solved numerically. It turns out that the number of acceptable roots, and hence the number of possible secondary beams, depends crucially on the frequency ratio ω_2/ω_1 and the angle ϕ which controls the obliqueness of the collision. Clearly, when the colliding beam with frequency ω_2 propagates upwards in z so the lower sign in (3.25) applies, $F^-_+(\psi) = 0$ has no acceptable roots as $\sin(\psi - \phi) > 0$, $\sin\psi > 0$ and $\sin\phi > 0$; thus, no secondary beams are found in $z > 0$. On the other hand, if the beam with frequency ω_2 is assumed to propagate downwards in z so the upper sign in (3.25) applies, two possibilities arise. First, if $\omega_2/\omega_1 < (1/2)$ $(\omega^- > \omega_2)$, one beam is found for each $0 < \phi < \pi$, as illustrated in figure 3(*a*) for $\theta_1 = 35°$, $\theta_2 = 14°$ $(\omega_1/\omega_2 = 0.422)$. Secondly, if $1/2 < \omega_2/\omega_1 < 1$ $(\omega^- < \omega_2)$, there is a critical value of $\phi = \phi_c$ above which no beams are found, but below which $F^-_-(\psi) = 0$ has two acceptable roots so that two secondary beams are possible, as illustrated in figure 3(*b*) for $\theta_1 = 35°$, $\theta_2 = 19°$ $(\omega_2/\omega_1 = 0.568)$.

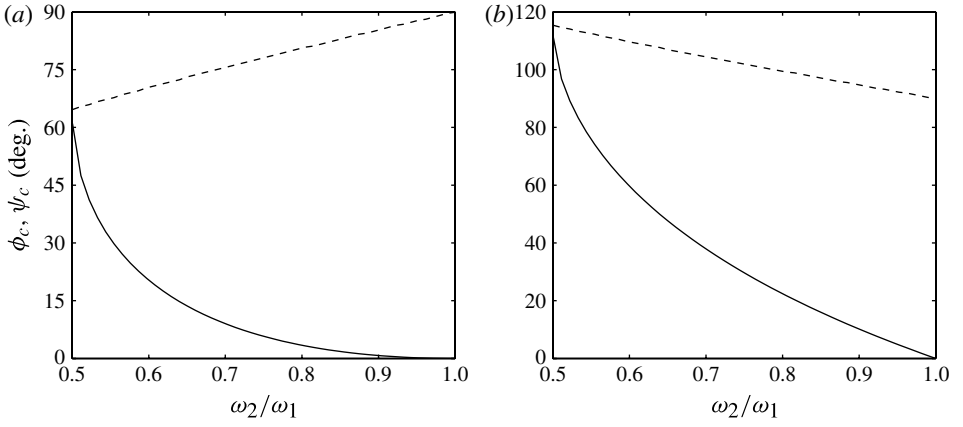

FIGURE 4. Critical obliqueness angle ϕ_c (—) of collision and corresponding obliqueness angle ψ_c (– –) of induced secondary beam with frequency ω^-, as the frequency ratio ω_2/ω_1 is varied: (*a*) beam radiating in $z > 0$; (*b*) beam radiating in $z < 0$. The colliding beams propagate at angles $\theta_1 = 35°$ and θ_2 in the range $16.666° < \theta_2 < \theta_1$ such that $1/2 < \omega_2/\omega_1 < 1$.

For waves that propagate in $z < 0$, the lower sign in (3.24) is appropriate, and (3.25) is replaced by

$$G^-_{\mp}(\psi) \equiv \cot\theta_1 \sin(\psi - \phi) \mp \cot\theta_2 \sin\psi - \sin\phi \cot\theta^- = 0. \tag{3.26}$$

In this instance, it turns out that there are no acceptable roots, and hence no beams are generated in $z < 0$, when the beam of frequency ω_2 propagates downwards in z, so the upper sign is valid in (3.26). If, however, this beam propagates upwards in z, again, depending on the frequency ratio ω_2/ω_1 and the obliqueness angle ϕ, there are two distinct scenarios: if $\omega_2/\omega_1 < 1/2$, one beam is generated in $z < 0$ for each $0 < \phi < \pi$, while if $1/2 < \omega_2/\omega_1 < 1$, either two or no beams arise, respectively, depending on whether ϕ is below or above a certain critical value ϕ_c. Figure 3(*c*,*d*) illustrates these two possibilities for $\theta_1 = 35°$, $\theta_2 = 14°$ ($\omega_2/\omega_1 = 0.422$) and $\theta_1 = 35°$, $\theta_2 = 19°$ ($\omega_2/\omega_1 = 0.568$).

Figure 4 shows how the collision obliqueness ϕ_c and the corresponding obliqueness angle ψ_c of the emitted beam at critical conditions vary with the frequency ratio ω_2/ω_1, for $\theta_1 = 35°$ and $16.666° < \theta_2 < 35°$. For each θ_2 in this range, two different ϕ_c are possible in general, corresponding to the case that the colliding beam of frequency $\omega_2 = \sin\theta_2$ propagates downwards or upwards in z and the radiated beam is found, respectively, in $z > 0$ (figure 4*a*) or $z < 0$ (figure 4*b*). In both of these configurations, ϕ_c decreases as ω_2/ω_1 is increased, with $\phi_c \to 0°$, $\psi_c \to 90°$ as $\omega_2/\omega_1 \to 1$. Also, in the other extreme, $\omega_2/\omega_1 \to 1/2$, it follows from (3.25) and (3.26) that ϕ_c and ψ_c approach a common value specified by $\cos\phi_c = \pm\cos\theta_1/(3 + \cos^2\theta_1)^{1/2}$, where the upper (lower) sign refers to the beam radiated in $z > 0$ ($z < 0$). It should be noted that the limit $\omega_2/\omega_1 \to 1$ is associated with hydrostatic beams ($\omega^- = 0$) and the limit $\omega_2/\omega_1 \to 1/2$ with subharmonic beams ($\omega^- = \omega_2 = (1/2)\omega_1$). As will be seen later (figure 7), close to these limiting collision configurations, the resonant response approaches zero.

The selection rules derived in Jiang & Marcus (2009) for plane collisions are deduced by combining (3.21) and (3.24) to solve for $\sin\psi/\sin\phi$ and $\sin(\psi - \phi)/\sin\phi$,

and then making use of (3.22) and (3.23) to ensure that $k_1 > 0$ and $k_2 > 0$. Carrying out this programme yields

$$\frac{\cos\psi\cot\theta_1 - \cot\theta^-}{\cot\theta_1\cos\phi \mp \cot\theta_2} > 0, \tag{3.27a}$$

$$\frac{-\cot\theta^-\cos\phi \pm \cot\theta_2\cos\psi}{\cot\theta_1\cos\phi \mp \cot\theta_2} > 0, \tag{3.27b}$$

and

$$\frac{\cos\psi\cot\theta_1 + \cot\theta^-}{\cot\theta_1\cos\phi \mp \cot\theta_2} > 0, \tag{3.28a}$$

$$\frac{\cot\theta^-\cos\phi \pm \cot\theta_2\cos\psi}{\cot\theta_1\cos\phi \mp \cot\theta_2} > 0, \tag{3.28b}$$

for wave beams with frequency ω^- radiating in $z > 0$ and $z < 0$, respectively. In both (3.27) and (3.28), the upper (lower) sign is to be used when the colliding beam of frequency ω_2 propagates downwards (upwards) in z. For plane collisions ($\phi = 0, \pi$), it is straightforward to check, on a case-by-case basis, whether these conditions can be satisfied when $\psi = 0$ or $\psi = \pi$, thus recovering the selection rules of Jiang & Marcus (2009).

Based on the above kinematic arguments, an interesting feature of oblique collisions when $\omega_2/\omega_1 > 1/2$ is the existence of a critical obliqueness, $\phi = \phi_c$, that marks the borderline between two or no secondary beams with frequency ω^- being radiated in the far field. Mathematically, $\phi = \phi_c$ is akin to a cut-off condition, as $\psi = \psi_c$ is a double root of $F_-^-(\psi) = 0$ in (3.25) or $G_+^-(\psi) = 0$ in (3.26), and the response switches from propagating to evanescent at $\phi = \phi_c$. As is well known, a similar situation arises in simpler wave propagation problems at cut-off frequencies. Also, as the group velocity is zero there, forced waves at cut-off frequencies feature unbounded steady-state amplitude owing to the accumulation of energy in the forcing region, and nonlinear effects are particularly important near such resonances (see, for example, Aranha *et al.* 1982 and Akylas 1984). In § 4 below, we shall compute the steady-state profiles of secondary beams resulting from oblique collisions and confirm that, here too, the amplitude of the beam of frequency ω^- becomes unbounded when $\phi = \phi_c$. A physical explanation of this resonance, in terms of the energy radiated by the beam of frequency ω^-, is presented in § 7.

4. Steady-state secondary beams

We now turn to a quantitative study of quadratic interactions between colliding wave beams, for the purpose of computing the amplitudes of the resulting secondary beams. To this end, following Tabaei *et al.* (2005), we introduce the perturbation expansions

$$\boldsymbol{u} = \epsilon\boldsymbol{u}^{(1)} + \epsilon^2\boldsymbol{u}^{(2)} + \cdots, \quad \rho = \epsilon\rho^{(1)} + \epsilon^2\rho^{(2)} + \cdots. \tag{4.1}$$

The leading-order terms represent the superposition of the two primary beams with frequencies ω_1 and ω_2 considered earlier (figure 1):

$$\boldsymbol{u}^{(1)} = \left\{\boldsymbol{U}_1(\eta_1)\mathrm{e}^{-\mathrm{i}\omega_1 t} + \text{c.c.}\right\} + \left\{\boldsymbol{U}_2(\eta_2)\mathrm{e}^{-\mathrm{i}\omega_2 t} + \text{c.c.}\right\}, \tag{4.2a}$$

$$\rho^{(1)} = \left\{R_1(\eta_1)\mathrm{e}^{-\mathrm{i}\omega_1 t} + \text{c.c.}\right\} + \left\{R_2(\eta_2)\mathrm{e}^{-\mathrm{i}\omega_2 t} + \text{c.c.}\right\}, \tag{4.2b}$$

$0 < \epsilon \ll 1$ being an amplitude parameter that controls the strength of these beams. (For example, we may define $\epsilon = U^*/N_0D^*$, in terms of the peak velocity U^* and the

characteristic width D^* of the beams, N_0 being the Brunt–Väisälä frequency.) In line with (2.8)–(2.10), the beam profiles

$$\boldsymbol{U}_1 = \int_0^\infty \hat{\boldsymbol{U}}_1(k_1)\mathrm{e}^{\mathrm{i}k_1\eta_1}\,\mathrm{d}k_1, \quad R_1 = \int_0^\infty \hat{R}(k_1)\mathrm{e}^{\mathrm{i}k_1\eta_1}\,\mathrm{d}k_1, \tag{4.3a}$$

$$\boldsymbol{U}_2 = \int_0^\infty \hat{\boldsymbol{U}}_2(k_2)\mathrm{e}^{\mathrm{i}k_2\eta_2}\,\mathrm{d}k_2, \quad R_2 = \int_0^\infty \hat{R}(k_2)\mathrm{e}^{\mathrm{i}k_2\eta_2}\,\mathrm{d}k_2, \tag{4.3b}$$

are functions of

$$\eta_1 = -x\sin\theta_1 + z\cos\theta_1, \quad \eta_2 = -x\sin\theta_2\cos\phi - y\sin\theta_2\sin\phi \pm z\cos\theta_2. \tag{4.4}$$

Also,

$$\hat{\boldsymbol{U}}_1 = A_1(k_1)(\cot\theta_1, 0, 1), \quad \hat{\boldsymbol{U}}_2 = A_2(k_2)(\pm\cot\theta_2\cos\phi, \pm\cot\theta_2\sin\phi, 1) \tag{4.5}$$

and

$$\hat{R}_1 = \frac{\mathrm{i}}{\sin\theta_1}A_1(k_1), \quad \hat{R}_2 = \frac{\mathrm{i}}{\sin\theta_2}A_2(k_2). \tag{4.6}$$

Note that, in keeping with the proper radiation conditions, the cross-beam coordinates (4.4) and the range of integration in (4.3) are consistent with the earlier choice of wavevectors $\boldsymbol{k}_1$ and $\boldsymbol{k}_2$ in (3.1). Also, as before, the upper (lower) sign in (4.4) and (4.5) applies when the beam with frequency ω_2 is taken to propagate downwards (upwards) in z.

Upon substituting (4.2) into the governing equations (2.1)–(2.3), quadratic interactions give rise to $O(\epsilon^2)$ terms with frequencies ω^+ and ω^-, which are confined within the region of overlap of the two colliding beams. These quadratic terms force $O(\epsilon^2)$ corrections, denoted by $\boldsymbol{u}^{(2)}$ and $\rho^{(2)}$ in (4.1), which, if permitted by the radiation conditions, propagate in the far field as secondary beams with frequencies ω^+ and ω^-.

To compute the $O(\epsilon^2)$ response, we shall employ (2.4), whose linear part involves the vertical velocity w and the right-hand side $\mathscr{R}$ comprises only nonlinear terms. Making use of the leading-order solution (4.2)–(4.6), it follows from (2.5) that

$$\mathscr{R} = \epsilon^2\{\mathscr{R}^+\mathrm{e}^{-\mathrm{i}\omega^+ t} + \text{c.c.}\} + \epsilon^2\{\mathscr{R}^-\mathrm{e}^{-\mathrm{i}\omega^- t} + \text{c.c.}\} + \cdots, \tag{4.7}$$

where

$$\mathscr{R}^+ = \mathrm{i}\nabla_H^2\left\{\left(\omega^+ + \frac{1}{\omega_2}\right)\boldsymbol{U}_1\cdot\nabla W_2 + \left(\omega^+ + \frac{1}{\omega_1}\right)\boldsymbol{U}_2\cdot\nabla W_1\right\}$$
$$- \mathrm{i}\omega^+\{\nabla_H\cdot(\boldsymbol{U}_1\cdot\nabla\boldsymbol{U}_{2H} + \boldsymbol{U}_2\cdot\nabla\boldsymbol{U}_{1H})\}_z, \tag{4.8a}$$

$$\mathscr{R}^- = \mathrm{i}\nabla_H^2\left\{\left(\omega^- - \frac{1}{\omega_2}\right)\boldsymbol{U}_1\cdot\nabla W_2^* + \left(\omega^- + \frac{1}{\omega_1}\right)\boldsymbol{U}_2^*\cdot\nabla W_1\right\}$$
$$- \mathrm{i}\omega^-\left\{\nabla_H\cdot(\boldsymbol{U}_1\cdot\nabla\boldsymbol{U}_{2H}^* + \boldsymbol{U}_2^*\cdot\nabla\boldsymbol{U}_{1H})\right\}_z, \tag{4.8b}$$

using the same notation as in (2.5) and with * denoting the complex conjugate. The correction to the vertical velocity, $w^{(2)}$, is then posed as

$$w^{(2)} = \{W^+\mathrm{e}^{-\mathrm{i}\omega^+ t} + \text{c.c.}\} + \{W^-\mathrm{e}^{-\mathrm{i}\omega^- t} + \text{c.c.}\}, \tag{4.9}$$

and, combining (2.4) with (4.7), $W^\pm$ satisfy

$$-\omega^{\pm 2}W_{zz}^\pm + \left(1 - \omega^{\pm 2}\right)\nabla_H^2 W^\pm = \mathscr{R}^\pm, \tag{4.10}$$

with $\omega^\pm = \sin\theta^\pm$.

The forced equations (4.10) are solved by transform methods, following the approach taken in Tabaei *et al.* (2005) for plane collisions. Briefly, taking the Fourier transform in x and y,

$$\widetilde{W}^{\pm}(k,l;z)=\frac{1}{4\pi^2}\int_{-\infty}^{\infty}\int_{-\infty}^{\infty}\mathrm{e}^{-\mathrm{i}(kx+ly)}W^{\pm}\,\mathrm{d}x\,\mathrm{d}y, \tag{4.11}$$

$$W^{\pm}(x,y,z)=\int_{-\infty}^{\infty}\int_{-\infty}^{\infty}\mathrm{e}^{\mathrm{i}(kx+ly)}\widetilde{W}^{\pm}\,\mathrm{d}k\,\mathrm{d}l, \tag{4.12}$$

where $\widetilde{W}^{\pm}$ satisfy

$$\widetilde{W}^{\pm}_{zz}+(k^2+l^2)\cot^2\theta^{\pm}\widetilde{W}^{\pm}=-\frac{\widetilde{\mathscr{R}}^{\pm}}{\sin^2\theta^{\pm}}. \tag{4.13}$$

Moreover, consistent with (3.12) and (3.24), $\widetilde{W}^{\pm}$ obey the radiation conditions

$$\widetilde{W}^{\pm}\sim\exp\{-\mathrm{i}\,(k^2+l^2)^{1/2}\cot\theta^{\pm}z\}\quad(z\to\infty), \tag{4.14a}$$

$$\widetilde{W}^{\pm}\sim\exp\{\mathrm{i}\,(k^2+l^2)^{1/2}\cot\theta^{\pm}z\}\quad(z\to-\infty). \tag{4.14b}$$

Equations (4.13) subject to (4.14) are readily solved by variation of parameters,

$$\begin{aligned}\widetilde{W}^{\pm}=\frac{-\mathrm{i}}{\sin 2\theta^{\pm}\kappa}\Bigg\{&\exp\left\{\mathrm{i}\kappa\cot\theta^{\pm}z\right\}\int_{z}^{\infty}\widetilde{R}^{\pm}(k,l;z')\exp\left\{-\mathrm{i}\kappa\cot\theta^{\pm}z'\right\}\,\mathrm{d}z'\\&+\exp\left\{-\mathrm{i}\kappa\cot\theta^{\pm}z\right\}\int_{-\infty}^{z}\widetilde{R}^{\pm}(k,l;z')\exp\left\{\mathrm{i}\kappa\cot\theta^{\pm}z'\right\}\,\mathrm{d}z'\Bigg\},\end{aligned} \tag{4.15}$$

where $\kappa=(k^2+l^2)^{1/2}$, and upon inserting (4.15) in (4.12), we obtain $W^{\pm}$. As our interest here is in radiating beams in the far field, we shall only quote the asymptotic expressions of $W^{\pm}$ as $|z|\to\infty$:

$$\begin{aligned}W^{\pm}\sim\frac{-\mathrm{i}}{\sin 2\theta^{\pm}}&\int_{-\infty}^{\infty}\int_{-\infty}^{\infty}\mathrm{d}k\,\mathrm{d}l\frac{\mathrm{e}^{\mathrm{i}(kx+ly)}}{\kappa}\exp\left\{-\mathrm{i}\kappa\cot\theta^{\pm}z\right\}\\&\times\int_{-\infty}^{\infty}\widetilde{\mathscr{R}}^{\pm}(k,l;z')\exp\left\{\mathrm{i}\kappa\cot\theta^{\pm}z'\right\}\,\mathrm{d}z'\quad(z\to\infty),\end{aligned} \tag{4.16a}$$

$$\begin{aligned}W^{\pm}\sim\frac{-\mathrm{i}}{\sin 2\theta^{\pm}}&\int_{-\infty}^{\infty}\int_{-\infty}^{\infty}\mathrm{d}k\,\mathrm{d}l\frac{\mathrm{e}^{\mathrm{i}(kx+ly)}}{\kappa}\exp\left\{\mathrm{i}\kappa\cot\theta^{\pm}z\right\}\\&\times\int_{-\infty}^{\infty}\widetilde{\mathscr{R}}^{\pm}(k,l;z')\exp\left\{-\mathrm{i}\kappa\cot\theta^{\pm}z'\right\}\,\mathrm{d}z'\quad(z\to-\infty).\end{aligned} \tag{4.16b}$$

We now compute $\widetilde{\mathscr{R}}^{\pm}$ in terms of the specific profiles (4.3) of the two colliding beams. Substituting (4.3) in (4.8), $\mathscr{R}^{\pm}$ can be written as

$$\mathscr{R}^{\pm}=\sum_{n=1}^{4}\mathscr{R}^{\pm}_{n}, \tag{4.17}$$

where each term in the above sum takes the form

$$\mathscr{R}^{\pm}_{n}=\int_{0}^{\infty}Q^{\pm}_{n}(k_1)\mathrm{e}^{\mathrm{i}k_1\eta_1}\,\mathrm{d}k_1\int_{0}^{\infty}S^{\pm}_{n}(k_2)\mathrm{e}^{\pm\mathrm{i}k_2\eta_2}\,\mathrm{d}k_2, \tag{4.18}$$

with $Q^{\pm}_{n}$ and $S^{\pm}_{n}$ being known functions that depend on the specific choices of $A_1(k_1)$ and $A_2(k_2)$ in (4.5). (Explicit expressions for $Q^{\pm}_{n}$ and $S^{\pm}_{n}$ are given in the Appendix.)

We shall first determine the contribution to the far-field response (4.16) of each term in (4.17) separately. Starting with $\mathscr{R}_n^+$, it follows from (4.18) and (4.4), upon performing the integrations over x and y in the Fourier transform defined in (4.11), that

$$\widetilde{\mathscr{R}}_n^+ = \frac{\mathrm{e}^{\mathrm{i}\alpha z}}{\sin\theta_1 \sin\theta_2 \sin\phi} Q_n^+ \left(\frac{l\cot\phi - k}{\sin\theta_1} \right) S_n^+ \left(-\frac{l}{\sin\theta_2 \sin\phi} \right), \tag{4.19}$$

where

$$\alpha = \cot\theta_1 (l\cot\phi - k) \mp l \frac{\cot\theta_2}{\sin\phi}, \tag{4.20}$$

and the upper (lower) sign holds when the beam of frequency ω_2 propagates downwards (upwards) in z. Also, in a similar way, one finds that the Fourier transform of $\mathscr{R}_n^-$ is

$$\widetilde{\mathscr{R}}_n^- = \frac{\mathrm{e}^{\mathrm{i}\alpha z}}{\sin\theta_1 \sin\theta_2 \sin\phi} Q_n^- \left(\frac{l\cot\phi - k}{\sin\theta_1} \right) S_n^- \left(\frac{l}{\sin\theta_2 \sin\phi} \right). \tag{4.21}$$

Upon inserting (4.19) and (4.21) in (4.16), the integration over z' in these expressions can be readily carried out, and collecting the contributions of all terms in (4.17) yields

$$W^\pm \sim \frac{-2\pi\mathrm{i}}{\sin\theta_1 \sin\theta_2 \sin\phi \sin 2\theta^\pm} \sum_{n=1}^{4} W_n^\pm, \tag{4.22}$$

where

$$W_n^\pm = \int_{-\infty}^{\infty}\int_{-\infty}^{\infty} \mathrm{d}k\,\mathrm{d}l \frac{\mathrm{e}^{\mathrm{i}(kx+ly)}}{\kappa} \mathscr{I}_n^\pm \exp\left\{-\mathrm{i}\kappa\cot\theta^\pm z\right\} \quad (z\to\infty), \tag{4.23a}$$

$$W_n^\pm = \int_{-\infty}^{\infty}\int_{-\infty}^{\infty} \mathrm{d}k\,\mathrm{d}l \frac{\mathrm{e}^{\mathrm{i}(kx+ly)}}{\kappa} \mathscr{J}_n^\pm \exp\left\{\mathrm{i}\kappa\cot\theta^\pm z\right\} \quad (z\to-\infty). \tag{4.23b}$$

Here,

$$\mathscr{I}_n^\pm = Q_n^\pm \left(\frac{l\cot\phi - k}{\sin\theta_1} \right) S_n^\pm \left(\mp\frac{l}{\sin\theta_2 \sin\phi} \right) \delta\left(\alpha + \kappa\cot\theta^\pm\right), \tag{4.24a}$$

$$\mathscr{J}_n^\pm = Q_n^\pm \left(\frac{l\cot\phi - k}{\sin\theta_1} \right) S_n^\pm \left(\mp\frac{l}{\sin\theta_2 \sin\phi} \right) \delta\left(\alpha - \kappa\cot\theta^\pm\right), \tag{4.24b}$$

where δ denotes the Dirac delta function and $\kappa = (k^2 + l^2)^{1/2}$.

It remains to carry out the integrations over k and l in (4.23). To this end, it is convenient to work with polar coordinates:

$$(k, l) = \kappa(\cos\chi, \sin\chi) \quad (0 \leqslant \kappa < \infty, 0 \leqslant \chi \leqslant 2\pi). \tag{4.25}$$

Note that, as $k_1 \geqslant 0$ and $k_2 \geqslant 0$ in (4.18), $Q_n^\pm$ and $S_n^\pm$ in (4.24) contribute to the integrals in (4.23) only when $l\cot\phi - k \geqslant 0$ and $\mp l \geqslant 0$; these conditions restrict χ in the range

$$\pi \leqslant \chi \leqslant \pi + \phi \tag{4.26}$$

for the response with frequency ω^+ (when the upper sign in (4.24) holds), and in the range

$$\phi \leqslant \chi \leqslant \pi \tag{4.27}$$

for the response with frequency ω^- (when the lower sign in (4.24) holds).

Using (4.25), the arguments of the delta functions in (4.24) may be expressed as

$$\alpha + \kappa \cot\theta^{\pm} = \frac{\kappa}{\sin\phi} F^{\pm}_{\mp}(\chi), \tag{4.28a}$$

$$\alpha - \kappa \cot\theta^{\pm} = \frac{\kappa}{\sin\phi} G^{\pm}_{\mp}(\chi), \tag{4.28b}$$

in terms of the functions $F^{\pm}_{\mp}$ and $G^{\pm}_{\mp}$ defined earlier in (3.13), (3.14), (3.25) and (3.26). Hence,

$$\delta\left(\alpha + \kappa \cot\theta^{\pm}\right) = \frac{\sin\phi}{\kappa \left|F^{\pm\prime}_{\mp}(\psi)\right|} \delta(\chi - \psi), \tag{4.29a}$$

$$\delta\left(\alpha - \kappa \cot\theta^{\pm}\right) = \frac{\sin\phi}{\kappa \left|G^{\pm\prime}_{\mp}(\psi)\right|} \delta(\chi - \psi), \tag{4.29b}$$

where ψ, generically, denotes the value(s), in the appropriate range (4.26) or (4.27), of χ for which the argument of each delta function in (4.24) vanishes. These ψ are precisely the roots of the equations $F^{\pm}_{\mp}(\psi) = 0$ and $G^{\pm}_{\mp}(\psi) = 0$ in (3.13), (3.14), (3.25) and (3.26), which determine the obliqueness relative to the xz-plane of possible secondary beams in the far field according to the earlier kinematic analysis. Also, the prime in (4.29) indicates the derivative of $F^{\pm}_{\mp}$ and $G^{\pm}_{\mp}$.

Finally, returning to (4.23) and performing the integration over χ, we obtain the far-field response. Specifically, from (4.22)–(4.24), making use of (4.25) and (4.29), the contribution of each root ψ to the far-field disturbance is a uniform beam

$$W^{\pm} \sim \int_0^{\infty} \hat{W}^{\pm}(k) \mathrm{e}^{\mathrm{i}k\eta^{\pm}} \,\mathrm{d}k, \tag{4.30}$$

whose profile depends on the cross-beam coordinate

$$\eta^{\pm} = x \sin\theta^{\pm} \cos\psi + y \sin\theta^{\pm} \sin\psi - z \cos\theta^{\pm} \quad (z > 0), \tag{4.31a}$$

$$\eta^{\pm} = x \sin\theta^{\pm} \cos\psi + y \sin\theta^{\pm} \sin\psi + z \cos\theta^{\pm} \quad (z < 0). \tag{4.31b}$$

Here,

$$\hat{W}^{\pm}(k) = -\frac{2\pi\mathrm{i}}{\sin\theta_1 \sin\theta_2 \sin 2\theta^{\pm}} \frac{1}{k \left|F^{\pm\prime}_{\mp}(\psi)\right|} \sum_{n=1}^{4} Q^{\pm}_n \left(k \frac{\sin\theta^{\pm} \sin(\psi - \phi)}{\sin\phi \sin\theta_1}\right) \times S^{\pm}_n \left(\mp k \frac{\sin\theta^{\pm} \sin\psi}{\sin\phi \sin\theta_2}\right) \quad (z \to \infty), \tag{4.32a}$$

$$\hat{W}^{\pm}(k) = -\frac{2\pi\mathrm{i}}{\sin\theta_1 \sin\theta_2 \sin 2\theta^{\pm}} \frac{1}{k \left|G^{\pm\prime}_{\mp}(\psi)\right|} \sum_{n=1}^{4} Q^{\pm}_n \left(k \frac{\sin\theta^{\pm} \sin(\psi - \phi)}{\sin\phi \sin\theta_1}\right) \times S^{\pm}_n \left(\mp k \frac{\sin\theta^{\pm} \sin\psi}{\sin\phi \sin\theta_2}\right) \quad (z \to -\infty). \tag{4.32b}$$

Based on (4.9) and (4.30)–(4.32), one may now compute the profiles of the radiated secondary beams in terms of the characteristics of the colliding beams. Here, ψ denotes the obliqueness angle of each radiated beam obtained from $F^{\pm}_{\mp}(\psi) = 0$

or $G_{\mp}^{\pm}(\psi) = 0$, consistent with the kinematic analysis in § 3. For oblique collisions at the critical angles $\phi = \phi_c$, in particular, where $\psi = \psi_c$ is a double root so $F_{-}^{-}(\psi_c) = F_{-}^{-'}(\psi_c) = 0$ or $G_{+}^{-}(\psi_c) = G_{+}^{-'}(\psi_c) = 0$, expressions (4.32) reveal that the steady-state amplitude of the radiated beam with frequency ω^- is unbounded. In § 6, we shall return to this resonance to examine the transient evolution of the response at critical conditions.

5. Numerical results

Here we report on sample computations of secondary beams due to oblique collisions, in an effort to shed light on how obliqueness influences the intensity of these beams. Specifically, we shall present numerical results for the energy flow rate associated with secondary beams. From Tabaei *et al.* (2005), the energy flow rate, averaged over a time period $2\pi/\omega$, in a uniform beam of the form (2.8)–(2.10) can be expressed as

$$\mathscr{F} = 4\pi \frac{\cot\theta}{\sin\theta} \int_0^\infty \frac{|A(k)|^2}{k}\, \mathrm{d}k. \tag{5.1}$$

Therefore, in view of (4.3), (4.9) and (4.30), the average energy flow rate in a secondary beam of frequency $\omega^\pm$, normalized with the average energy flow rate in the colliding beam of frequency ω_1, is $\epsilon^2 \mathscr{F}^\pm$, where

$$\mathscr{F}^\pm = \frac{\cot\theta^\pm \sin\theta_1}{\cot\theta_1 \sin\theta^\pm} \frac{\displaystyle\int_0^\infty |\hat{W}^\pm(k)|^2\, \mathrm{d}k/k}{\displaystyle\int_0^\infty |A_1(k)|^2\, \mathrm{d}k/k}, \tag{5.2}$$

with $\hat{W}^\pm(k)$ given by (4.32).

The two colliding wave beams are taken to have the same Gaussian streamfunction profiles as in Tabaei *et al.* (2005), which translates to the choices

$$A_1(k_1) = \mathrm{i}\sqrt{\frac{1}{8\pi}}\, \sin\theta_1 k_1 \mathrm{e}^{-k_1^2/8}, \quad A_2(k_2) = \mathrm{i}\sqrt{\frac{1}{8\pi}}\, \sin\theta_2 k_2 \mathrm{e}^{-k_2^2/8} \tag{5.3}$$

for the spectral amplitudes in (4.5). Based on the expressions given in the Appendix, it is then straightforward to compute the functions $Q_n^\pm$ and $S_n^\pm$ in (4.32) and thereby $\mathscr{F}^\pm$ in (5.2).

Figure 5 shows plots of the average energy flow rate $\mathscr{F}^+$ in radiated beams of frequency ω^+, as a function of the angle $0° < \phi < 180°$ that controls the obliqueness of the collision, for $\theta_1 = 35°$ and θ_2 in the range $0° < \theta_2 < 24.41°$ where $0 < \omega^+ < 1$. As ϕ is varied, for both the beam radiated in $z > 0$ (figure 5*a*) and the beam radiated in $z < 0$ (figure 5*b*), the maximum of $\mathscr{F}^+$ is realized for a plane collision ($\phi = 0°$ or $\phi = 180°$). Also, it is interesting that the energy flow rate in the beam radiated in $z < 0$ can be nearly zero, and this minimum occurs when ϕ is roughly 90° irrespective of the incidence angle θ_2, as indicated in figure 5(*b*).

Similar overall behaviour is exhibited by the average energy flow rate $\mathscr{F}^-$ associated with radiated beams of frequency ω^-, in the case $0 < \omega_2/\omega_1 < 1/2$ where no resonances are possible. Figure 6 shows plots of $\mathscr{F}^-$ as a function of ϕ for $\theta_1 = 35°$ and $0° < \theta_2 < 16.666°$ where $0 < \omega_2/\omega_1 < 1/2$. Again, for each θ_2 in this range, the maximum $\mathscr{F}^-$ arises at a plane collision ($\phi = 0°$ or $\phi = 180°$) for both the beam found in $z > 0$ (figure 6*a*) and the beam found in $z < 0$ (figure 6*b*). It is

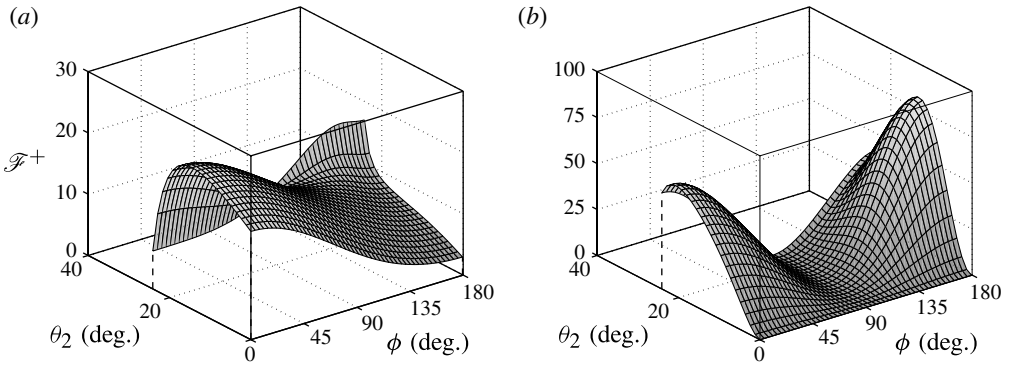

FIGURE 5. Average energy flow rate $\mathscr{F}^+$ associated with induced secondary beam of frequency ω^+, as a function of the angle $0° < \phi < 180°$ that controls the obliqueness of the collision (see figure 1): (*a*) beam radiating in $z > 0$; (*b*) beam radiating in $z < 0$. The colliding beams propagate at angles $\theta_1 = 35°$ and $0° < \theta_2 < 24.41°$ such that $\omega^+ < 1$.

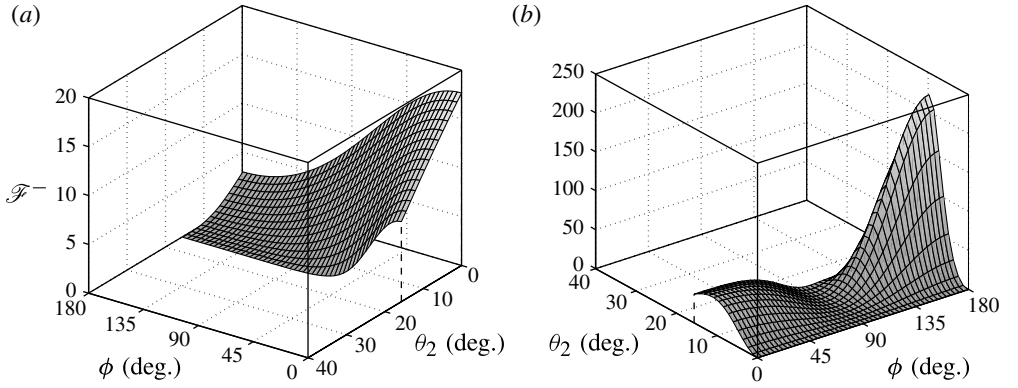

FIGURE 6. Average energy flow rate $\mathscr{F}^-$ associated with induced secondary beam of frequency ω^-, as a function of the angle $0° < \phi < 180°$ that controls the obliqueness of the collision (see figure 1): (*a*) beam radiating in $z > 0$; (*b*) beam radiating in $z < 0$. The colliding beams propagate at angles $\theta_1 = 35°$ and $0° < \theta_2 < 16.666°$ such that $0 < \omega_2/\omega_1 < 1/2$; in this frequency range, no resonances are possible.

worth noting that the maximum $\mathscr{F}^-$ in the latter case is significantly larger than in the former; however, $\mathscr{F}^-$ for the beam found in $z < 0$ again turns out to be nearly zero for oblique collisions with ϕ around 90°, regardless of the incidence angle θ_2.

The results presented above for the incidence angle $\theta_1 = 35°$ are typical of secondary beams with frequency ω^+, and of secondary beams with frequency ω^- in the case that the frequency ratio of the colliding beams is in the range $0 < \omega_2/\omega_1 < 1/2$. When $1/2 < \omega_2/\omega_1 < 1$, though, $\mathscr{F}^-$ is dominated by the resonances that occur for oblique collisions at critical conditions. We shall return to this issue at the end of § 6.

6. Resonant collision

As remarked in § 4, when the frequencies of the colliding wave beams are such that $1/2 < \omega_2/\omega_1 < 1$, the steady-state amplitude of the induced beam with frequency $\omega^- = \omega_1 - \omega_2$ is unbounded for certain oblique collision configurations. To clarify the

nature of this resonance phenomenon, we now examine the transient evolution of the $O(\epsilon^2)$ radiated disturbance at critical conditions.

Returning to (2.4), the portion of the forcing term $\mathscr{R}$ in (4.7) with frequency ω^-, $\epsilon^2\{\mathscr{R}^-\mathrm{e}^{-\mathrm{i}\omega^- t}+\text{c.c.}\}$, is assumed to be switched on impulsively at $t=0$. The induced $O(\epsilon^2)$ perturbation to the vertical velocity, $\epsilon^2\{w^-+\text{c.c.}\}$, is then governed by

$$\nabla^2 w^-_{tt}+\nabla_H^2 w^- = \mathscr{R}^-\mathrm{e}^{-\mathrm{i}\omega^- t} \quad (t>0), \tag{6.1a}$$

$$w^- = w^-_t = 0 \quad (t=0), \tag{6.1b}$$

assuming that the motion starts from rest. This initial-value problem mimics, albeit in a rough sense, the gradual development of disturbances with frequency ω^-, following the collision of the two primary beams at $t=0$. Compared with the steady-state analysis of § 4, the present approach, while mathematically more involved, has the advantage that it is also applicable at critical obliqueness where the steady-state response is singular.

The problem (6.1) is solved by taking Fourier transform in x, y and z,

$$\tilde{\tilde{w}}^-(k,l,m;t)=\frac{1}{2\pi}\int_{-\infty}^{\infty}\mathrm{e}^{-\mathrm{i}mz}\tilde{w}^-\,\mathrm{d}z, \tag{6.2}$$

$\tilde{w}^-(k,l;z,t)$ being the Fourier transform in x and y as defined in (4.11), so

$$w^-(x,y;z,t)=\int_{-\infty}^{\infty}\int_{-\infty}^{\infty}\int_{-\infty}^{\infty}\mathrm{e}^{\mathrm{i}(kx+ly+mz)}\tilde{\tilde{w}}^-\,\mathrm{d}k\,\mathrm{d}l\,\mathrm{d}m. \tag{6.3}$$

Thus, $\tilde{\tilde{w}}^-$ satisfies

$$\tilde{\tilde{w}}^-_{tt}+\Omega^2\tilde{\tilde{w}}^- = -\frac{\tilde{\tilde{\mathscr{R}}}^-}{|\boldsymbol{k}|^2}\mathrm{e}^{-\mathrm{i}\omega^- t} \quad (t>0), \tag{6.4a}$$

$$\tilde{\tilde{w}}^- = \tilde{\tilde{w}}^-_t = 0 \quad (t=0), \tag{6.4b}$$

where

$$\Omega^2=\frac{k^2+l^2}{|\boldsymbol{k}|^2}, \tag{6.5}$$

with $|\boldsymbol{k}|^2\equiv k^2+l^2+m^2$. Solving (6.4) for $\tilde{\tilde{w}}^-$ then yields

$$\tilde{\tilde{w}}^-=\frac{\tilde{\tilde{\mathscr{R}}}^-}{|\boldsymbol{k}|^2}\left\{\frac{\mathrm{e}^{-\mathrm{i}\omega^- t}}{\omega^{-2}-\Omega^2}+\frac{1}{2\Omega}\left(\frac{\mathrm{e}^{\mathrm{i}\Omega t}}{\omega^-+\Omega}-\frac{\mathrm{e}^{-\mathrm{i}\Omega t}}{\omega^--\Omega}\right)\right\}. \tag{6.6}$$

Here, in view of (4.17) and (4.21),

$$\tilde{\tilde{\mathscr{R}}}^-=\sum_{n=1}^{4}\tilde{\tilde{\mathscr{R}}}^-_n \tag{6.7}$$

where

$$\tilde{\tilde{\mathscr{R}}}^-_n=\frac{1}{\sin\theta_1\sin\theta_2\sin\phi}Q_n^-\left(\frac{l\cot\phi-k}{\sin\theta_1}\right)S_n^-\left(\frac{l}{\sin\theta_2\sin\phi}\right)\delta(m-\alpha), \tag{6.8}$$

and α is given in (4.20).

We now invert the Fourier transform $\tilde{\tilde{w}}^-$ to obtain w^- according to (6.3). Inserting (6.6) in (6.3) and performing first the integration over m, we find

$$\tilde{w}^- = \sum_{n=1}^{4} \tilde{w}_n^-, \tag{6.9}$$

where

$$\tilde{w}_n^- = \frac{\tilde{\tilde{\mathscr{R}}}_n^-}{k^2 + l^2 + \alpha^2} \left\{ \frac{\mathrm{e}^{-\mathrm{i}\omega^- t}}{\omega^{-2} - \tilde{\Omega}^2} + \frac{1}{2\tilde{\Omega}} \left(\frac{\mathrm{e}^{\mathrm{i}\tilde{\Omega} t}}{\omega^- + \tilde{\Omega}} - \frac{\mathrm{e}^{-\mathrm{i}\tilde{\Omega} t}}{\omega^- - \tilde{\Omega}} \right) \right\}, \tag{6.10}$$

with

$$\tilde{\Omega}^2 = \frac{k^2 + l^2}{k^2 + l^2 + \alpha^2}, \tag{6.11}$$

and $\tilde{\tilde{\mathscr{R}}}_n^-$ is given in (4.21). Next, to carry out the integrations over k and l, we introduce polar coordinates (κ, χ) according to (4.25), with χ again in the range $\phi \leqslant \chi \leqslant \pi$ so that the arguments of Q_n^- and S_n^- in expression (4.21) for $\tilde{\tilde{\mathscr{R}}}_n^-$ are positive. After some algebra, it is found that

$$w^- = \sum_{n=1}^{4} w_n^-, \tag{6.12}$$

where

$$\begin{aligned} w_n^- = \frac{\sin\phi}{\sin\theta_1 \sin\theta_2} \int_0^\infty \frac{\mathrm{d}\kappa}{\kappa} \int_\phi^\pi \mathrm{d}\chi \exp\left\{ \mathrm{i}\kappa \left(x\cos\chi + y\sin\chi + z\frac{\tilde{\alpha}}{\sin\phi} \right) \right\} \\ \times Q_n^- \left(\kappa \frac{\sin(\chi - \phi)}{\sin\theta_1 \sin\phi} \right) S_n^- \left(\kappa \frac{\sin\chi}{\sin\theta_2 \sin\phi} \right) \frac{1}{(\tilde{\alpha}^2 + \sin^2\phi)} \\ \times \left\{ \frac{\mathrm{e}^{-\mathrm{i}\omega^- t}}{\omega^{-2} - \tilde{\Omega}^2} + \frac{1}{2\tilde{\Omega}} \left(\frac{\mathrm{e}^{\mathrm{i}\tilde{\Omega} t}}{\omega^- + \tilde{\Omega}} - \frac{\mathrm{e}^{-\mathrm{i}\tilde{\Omega} t}}{\omega^- - \tilde{\Omega}} \right) \right\}, \end{aligned} \tag{6.13}$$

with

$$\tilde{\Omega}^2 = \frac{\sin^2\phi}{\sin^2\phi + \tilde{\alpha}^2} \tag{6.14}$$

and

$$\tilde{\alpha} = \frac{\sin\phi}{\kappa}\alpha = \cot\theta_1 \sin(\chi - \phi) \mp \cot\theta_2 \sin\chi. \tag{6.15}$$

Formally, of the three time-dependent terms in the curly brackets in expression (6.13), the term proportional to $\mathrm{e}^{-\mathrm{i}\omega^- t}$ corresponds to the result of the steady-state analysis, while the terms that involve $\mathrm{e}^{\pm\mathrm{i}\tilde{\Omega} t}$ derive from satisfying the initial conditions (6.1*b*). As indicated below, however, separating the response into steady-state and transient components requires careful interpretation of the various integrals in (6.13).

Consider first the integral over χ in (6.13). Attention is focused on possible zeros on the real χ-axis of the denominators of the terms in the curly brackets. Within the integration range $\phi \leqslant \chi \leqslant \pi$, such zeros are associated with poles of the integrand on the integration path, which are key to determining the far-field response in forced wave

problems (see, for example, Lighthill 1978, § 4.9). Specifically, making use of (6.14) and (6.15), the denominator of the term involving $\mathrm{e}^{-\mathrm{i}\omega^- t}$ in (6.13) can be written as

$$\omega^{-2} - \tilde{\Omega}^2 = \frac{\sin^2\theta^-}{\sin^2\phi + \tilde{\alpha}^2}\left(\tilde{\alpha}^2 - \sin^2\phi\cot^2\theta^-\right). \tag{6.16}$$

Hence, the zeros of interest here are the real roots, within the range $\phi \leqslant \chi \leqslant \pi$, of

$$\tilde{\alpha}^2 - \sin^2\phi\cot^2\theta^- = F_{\mp}^-(\chi)G_{\mp}^-(\chi) = 0, \tag{6.17}$$

$F_{\mp}^-$ and $G_{\mp}^-$ being the functions encountered earlier in (3.25) and (3.26); these zeros thus coincide with the roots $\chi = \psi$ of $F_{\mp}^-(\psi) = 0$ and $G_{\mp}^-(\psi) = 0$, which determine the obliqueness relative to the xz-plane of steady-state beams found in $z > 0$ and $z < 0$, respectively. Note that, at $\chi = \psi$, the term proportional to $\mathrm{e}^{-\mathrm{i}\omega^- t}$ in (6.13) has a pole on the integration path and the corresponding integral, on its own, is singular. This difficulty stems from the fact that the steady-state response is not well defined if no suitable radiation conditions are imposed. On the other hand, as a whole, the integral over χ in (6.13) is not singular because the pole at $\chi = \psi$ of the term involving $\mathrm{e}^{-\mathrm{i}\omega^- t}$ is cancelled by the other terms in the curly brackets.

In order to extract the steady-state far-field response from the full unsteady solution (6.12)–(6.13), one may first deform the integration path in (6.13) away from the real χ-axis so that the integrals over χ corresponding to each of the terms in the curly brackets are no longer singular, and then evaluate these integrals by residue calculus and the method of stationary phase. Details of this rather lengthy procedure will not be pursued here, as the secondary beams radiated in the far field were obtained more directly in § 4 from the steady-state solution after imposing suitable radiation conditions. We shall make use of the unsteady solution (6.12)–(6.13), though, to examine the asymptotic behaviour of the far-field disturbance under resonant conditions, where the steady-state analysis breaks down.

As noted earlier, at critical obliqueness ($\phi = \phi_c$), $F_-^-(\psi) = 0$ in (3.25) or $G_+^-(\psi) = 0$ in (3.26) has a double root, $\psi = \psi_c$, so $F_-^{-\prime}(\psi_c) = 0$ or $G_+^{-\prime}(\psi_c) = 0$ as well. As a result, the terms involving $\mathrm{e}^{-\mathrm{i}\omega^- t}$ and $\mathrm{e}^{-\mathrm{i}\tilde{\Omega}t}$ in (6.13) feature a double pole at $\chi = \psi_c$:

$$\omega^{-2} - \tilde{\Omega}^2 = -\sin^2\theta^-\cos^2\theta^-\,(\chi - \psi_c)^2 + \cdots, \tag{6.18}$$

$$\omega^- - \tilde{\Omega} = -\tfrac{1}{2}\sin\theta^-\cos^2\theta^-(\chi - \psi_c)^2 + \cdots. \tag{6.19}$$

Moreover, since

$$\left.\frac{\partial\tilde{\Omega}}{\partial\chi}\right|_c = \left.\frac{\partial\tilde{\alpha}}{\partial\chi}\right|_c = 0, \tag{6.20}$$

$\chi = \psi_c$ is a point of stationary phase when the integrals over χ in (6.13) are evaluated asymptotically in the far field, $t \to \infty$ and $|z| \to \infty$. An analogous situation, where a double pole coincides with a point of stationary phase, arises in a classical problem of water waves, namely in the disturbance induced by a moving external pressure distribution oscillating at resonant frequency. In this simpler setting, the far-field behaviour of the resonant response is deduced from the integral representation of the full unsteady solution by expanding the integrand in the neighbourhood of the double pole (Akylas 1984).

Taking a similar approach here, it is argued that the dominant contribution to the integral over χ in (6.13) at critical obliqueness ($\phi = \phi_c$) comes from the

neighbourhood of $\chi = \psi_c$. Accordingly, setting $\chi = \psi_c + s$ and using (6.18)–(6.20), the various parts of the integrand are expanded around $s = 0$ as follows:

$$\exp\left\{\mathrm{i}\kappa\left(x\cos\chi + y\sin\chi + z\frac{\tilde{\alpha}}{\sin\phi_c}\right)\right\} = \exp\left(\mathrm{i}\kappa\eta_c^-/\sin\theta^-\right) \times \exp\left\{\mathrm{i}\kappa s\left(-x\sin\psi_c + y\cos\psi_c\right)\right\} + \cdots, \tag{6.21}$$

where

$$\eta_c^- = x\sin\theta^-\cos\psi_c + y\sin\theta^-\sin\psi_c \mp z\cos\theta^- \quad (z \gtrless 0) \tag{6.22}$$

denotes the cross-beam coordinate of a beam of frequency ω^- and obliqueness ψ_c radiated in $z \gtrless 0$;

$$Q_n^-\left(\kappa\frac{\sin(\chi-\phi_c)}{\sin\theta_1\sin\phi_c}\right)S_n^-\left(\kappa\frac{\sin\chi}{\sin\theta_2\sin\phi_c}\right)\frac{1}{\left(\tilde{\alpha}^2+\sin^2\phi_c\right)} = \frac{\sin^2\theta^-}{\sin^2\phi_c}Q_n^-\left(\kappa\frac{\sin(\psi_c-\phi_c)}{\sin\theta_1\sin\phi_c}\right)S_n^-\left(\kappa\frac{\sin\psi_c}{\sin\theta_2\sin\phi_c}\right)+\cdots; \tag{6.23}$$

$$\frac{\mathrm{e}^{-\mathrm{i}\omega^- t}}{\omega^{-2}-\tilde{\Omega}^2} = -\frac{\mathrm{e}^{-\mathrm{i}\omega^- t}}{\sin^2\theta^-\cos^2\theta^-}\frac{1}{s^2}+\cdots; \tag{6.24}$$

and finally

$$\frac{\mathrm{e}^{-\mathrm{i}\tilde{\Omega}t}}{2\tilde{\Omega}\left(\omega^- - \tilde{\Omega}\right)} = -\frac{\mathrm{e}^{-\mathrm{i}\omega^- t}}{\sin^2\theta^-\cos^2\theta^-}\frac{\exp\left(-\frac{\mathrm{i}}{2}\sin\theta^-\cos^2\theta^- s^2 t\right)}{s^2}+\cdots. \tag{6.25}$$

Combining (6.21)–(6.25) with (6.13), we thus find

$$w_n^- \sim \frac{\mathrm{e}^{-\mathrm{i}\omega^- t}}{\sin\theta_1\sin\theta_2\cos^2\theta^-\sin\phi_c} \times \int_0^\infty \frac{\mathrm{d}\kappa}{\kappa}\exp\left(\mathrm{i}\kappa\eta_c^-/\sin\theta^-\right)Q_n^-\left(\kappa\frac{\sin(\psi_c-\phi_c)}{\sin\theta_1\sin\phi_c}\right)S_n^-\left(\kappa\frac{\sin\psi_c}{\sin\theta_2\sin\phi_c}\right) \times \int_{-\infty}^\infty \frac{\mathrm{d}s}{s^2}\exp\left\{\mathrm{i}\kappa s\left(-x\sin\psi_c + y\cos\psi_c\right)\right\} \times \left\{\exp\left(-\frac{\mathrm{i}}{2}\sin\theta^-\cos^2\theta^- s^2 t\right) - 1\right\}. \tag{6.26}$$

Note that, in line with the stationary-phase approximation, the integration over s in (6.26) extends from $-\infty$ to ∞; as the main contribution to this integral comes from the vicinity of the stationary point $s = 0$ where (6.21)–(6.25) are valid, the rest of the integration range is relatively unimportant.

To interpret the far-field disturbance, it is helpful to replace the integration variable s in (6.26) with

$$\sigma = st^{1/2}. \tag{6.27}$$

After some manipulation, it then follows from (6.12) and (6.26) that the overall response $\{w^- + \text{c.c.}\}$ takes the form

$$\{w^- + \text{c.c.}\} \sim t^{1/2} \mathrm{e}^{-\mathrm{i}\omega^- t} \int_0^\infty \hat{W}_c^-(k;\xi) \mathrm{e}^{\mathrm{i}k\eta_c^-}\, \mathrm{d}k + \text{c.c.}, \tag{6.28}$$

where

$$\hat{W}_c^- = \frac{1}{\sin\theta_1 \sin\theta_2 \cos^2\theta^- \sin\phi_c} \frac{J(k;\xi)}{k} \times \sum_{n=1}^{4} Q_n^- \left(k \frac{\sin\theta^- \sin(\psi_c - \phi_c)}{\sin\theta_1 \sin\phi_c} \right) S_n^- \left(k \frac{\sin\theta^- \sin\psi_c}{\sin\theta_2 \sin\phi_c} \right). \tag{6.29}$$

Here

$$J = \int_{-\infty}^{\infty} \frac{\mathrm{d}\sigma}{\sigma^2} \exp\left(\mathrm{i}k\sigma\xi \sin\theta^-\right) \left\{ \exp\left(-\frac{\mathrm{i}}{2} \sin\theta^- \cos^2\theta^- \sigma^2 \right) - 1 \right\}, \tag{6.30}$$

with

$$\xi = \frac{-x \sin\psi_c + y \cos\psi_c}{t^{1/2}}. \tag{6.31}$$

According to (6.28), the far-field response at $\phi = \phi_c$ is a beam-like disturbance with constant frequency ω^- and obliqueness ψ_c relative to the xz-plane, but varying profile and amplitude. Similarly to forced waves at a cut-off frequency (Aranha *et al.* 1982; Akylas 1984), the beam amplitude grows in time like $t^{1/2}$, which explains the unbounded response found in the steady-state analysis in § 4. This resonant behaviour can be traced back to conditions (6.20) at $\phi = \phi_c$, which are analogous to the group velocity being zero at cut-off frequencies (see also § 7 below for a physical interpretation of the resonance conditions in the present setting). Moreover, the beam profile in (6.28) is not only a function of the cross-beam coordinate η_c^-, but also evolves spatially and temporally in a self-similar fashion via ξ in (6.31); this similarity variable accounts for the presence of slow modulations in the transverse direction. At any fixed position, the modulations eventually disperse out, since $\xi \to 0$ as $t \to \infty$, and $J(\kappa;\xi)$ in (6.30) approaches a constant:

$$J_0 = \int_{-\infty}^{\infty} \frac{\mathrm{d}\sigma}{\sigma^2} \left\{ \exp\left(-\frac{\mathrm{i}}{2} \sin\theta^- \cos^2\theta^- \sigma^2 \right) - 1 \right\} = -\sqrt{\pi}(\mathrm{i}+1)\sqrt{\sin\theta^-}\cos\theta^-. \tag{6.32}$$

As a result, after a long time, the resonant response locally tends to a plane beam with uniform profile, while the amplitude continuously grows in time like $t^{1/2}$.

From these findings, the average energy flow rate in the emitted resonant wave beam, normalized with the average energy flow rate in the colliding beam of frequency ω_1, is expected to grow linearly with time, like $\epsilon^2 \mathscr{F}_c^- t$. We may estimate $\mathscr{F}_c^-$ based on (5.2) by replacing $\hat{W}^-(k)$ with $\hat{W}_c^-(k;\xi=0)$, as given by (6.29) with $J = J_0$ according to (6.32). Figure 7 shows $\mathscr{F}_c^-$ corresponding to the critical angles ϕ_c displayed in figure 4, for $1/2 < \omega_2/\omega_1 < 1$. The colliding beams are taken to have the same Gaussian profiles as in (5.3). Both plots in figure 7 are bell-shaped curves, approaching zero in the subharmonic ($\omega_2/\omega_1 \to 1/2$) and the hydrostatic ($\omega_2/\omega_1 \to 1$) limits. The peak value of $\mathscr{F}_c^-$ is found at $\omega_2/\omega_1 = 0.563$ ($\phi_c = 27.61°$) for the beam

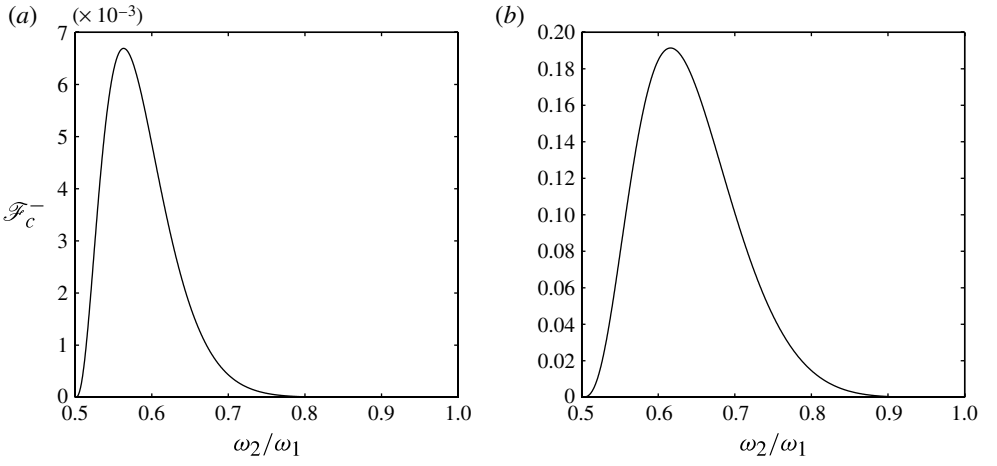

FIGURE 7. Normalized energy flow rate $\mathscr{F}_c^-$ associated with secondary beam due to resonant oblique collisions at the critical angles ϕ_c displayed in figure 4, as the frequency ratio ω_2/ω_1 is varied: (*a*) beam radiating in $z > 0$; (*b*) beam radiating in $z < 0$. The colliding beams propagate at angles $\theta_1 = 35°$ and θ_2 in the range $16.666° < \theta_2 < \theta_1$ such that $1/2 < \omega_2/\omega_1 < 1$.

radiated in $z > 0$ (figure 7*a*) and at $\omega_2/\omega_1 = 0.616$ ($\phi_c = 55.49°$) for the beam radiated in $z < 0$ (figure 7*b*). It should be noted that in the latter case the response curve is broader and the corresponding peak significantly taller than in the former case, indicating that the resonance associated with the beam radiated in $z < 0$ is relatively stronger. We recall that, in the range $0 < \omega_2/\omega_1 < 1/2$ where no resonances are possible, the steady-state beam radiated in $z < 0$ again typically turns out to be stronger than the one radiated in $z > 0$ (figure 6).

7. Physical interpretation of resonance

Based on the above mathematical analysis of oblique beam collisions, resonance occurs when the obliqueness angle of an emitted secondary beam with frequency ω^-, happens to be a double root, $\psi = \psi_c$, of equation $F_-^-(\psi) = 0$ in (3.25) or $G_+^-(\psi) = 0$ in (3.26), so $F_-^{-\prime}(\psi_c) = 0$ or $G_+^{-\prime}(\psi_c) = 0$, respectively. These resonance conditions may be understood on physical grounds by examining the transport of energy due to the generated beam at resonance.

Returning to the kinematic considerations in § 3.2, a secondary beam of frequency ω^- and obliqueness ψ comprises plane waves with wavevectors $\boldsymbol{k}^-$, determined from (3.20) together with (3.21) and (3.24)–(3.26). These wavevectors point in the same direction, and the resulting beam propagates along

$$\boldsymbol{d}^- = \boldsymbol{k}^- \times (\boldsymbol{k}^- \times \hat{\boldsymbol{e}}_z), \tag{7.1}$$

where $\hat{\boldsymbol{e}}_z$ denotes a vertical unit vector pointing upwards. Recall that the along-beam direction $\boldsymbol{d}^-$, as it is parallel to $\boldsymbol{c}_g^-$, is also the direction in which energy is transported by the beam.

As remarked earlier, secondary beams are generated by quadratic nonlinear interactions of the two colliding primary beams in the region where these beams

meet. This overlap region, which acts as the wave source, stretches along

$$\boldsymbol{d}^s = \boldsymbol{k}_1 \times \boldsymbol{k}_2, \tag{7.2}$$

$\boldsymbol{k}_1$ and $\boldsymbol{k}_2$ being the wavevectors (3.1) partaking in the primary beams. For given beam frequencies ω_1 and ω_2 and obliqueness angle of the collision ϕ, the directions of $\boldsymbol{k}_1$ and $\boldsymbol{k}_2$, and hence $\boldsymbol{d}^s$, are fixed.

We shall demonstrate that, in a resonant collision,

$$\boldsymbol{d}^- \times \boldsymbol{d}^s = 0, \tag{7.3}$$

implying that the generated beam of frequency ω^- propagates along the direction of the source. Under resonant conditions, therefore, energy cannot escape from the forcing region, causing the beam amplitude to grow in time continuously.

To prove (7.3) at resonance, using (7.1), (7.2) and standard vector identities, we find

$$\boldsymbol{d}^- \times \boldsymbol{d}^s = B_1 \boldsymbol{k}^- + B_2(\boldsymbol{k}^- \times \hat{\boldsymbol{e}}_z), \tag{7.4}$$

where

$$B_1 = (\boldsymbol{k}_2 \cdot \boldsymbol{k}^-)(\boldsymbol{k}_1 \cdot \hat{\boldsymbol{e}}_z) - (\boldsymbol{k}_1 \cdot \boldsymbol{k}^-)(\boldsymbol{k}_2 \cdot \hat{\boldsymbol{e}}_z), \tag{7.5a}$$

$$B_2 = \boldsymbol{k}^- \cdot (\boldsymbol{k}_1 \times \boldsymbol{k}_2). \tag{7.5b}$$

Since $\boldsymbol{k}^- = \boldsymbol{k}_1 - \boldsymbol{k}_2$ in view of (3.4), however, $B_2 = 0$. Moreover, using (3.1), (3.20), (3.21) and (3.24), B_1 can be expressed as

$$B_1 = k_1 k_2 \kappa \sin\theta_1 \sin\theta_2 \sin\theta^- (\pm \cot\theta_2 \cos\psi - \cot\theta_1 \cos(\psi - \phi)), \tag{7.6}$$

where the upper (lower) sign is valid for beams of frequency ω^- radiating in $z > 0$ ($z < 0$). Finally, recalling (3.25) and (3.26), it follows from (7.6) that

$$B_1 = -k_1 k_2 \kappa \sin\theta_1 \sin\theta_2 \sin\theta^- F_-^{-\prime}(\psi) \quad (z > 0), \tag{7.7a}$$

$$B_1 = -k_1 k_2 \kappa \sin\theta_1 \sin\theta_2 \sin\theta^- G_+^{-\prime}(\psi) \quad (z < 0). \tag{7.7b}$$

This establishes that $B_1 = 0$ at a resonant obliqueness $\psi = \psi_c$, where $F_-^{-\prime}(\psi_c) = 0$ ($z > 0$) or $G_+^{-\prime}(\psi_c) = 0$ ($z < 0$), and hence (7.3) holds at resonance.

8. Concluding remarks

We have studied collisions of weakly nonlinear internal wave beams and the attendant radiation of secondary beams due to quadratic nonlinear interactions, in the general case where the colliding beams propagate in different vertical planes. Based on wave kinematics and suitable radiation conditions, the propagation directions of radiated beams in such oblique collisions were determined. We have also explored the effects of obliqueness of a collision on the strength of radiated beams. Sample computations indicate that, typically, the strongest secondary beams arise for a plane collision of two beams. However, for certain oblique collision configurations, the induced secondary beam with frequency equal to the difference of those of the colliding beams has unbounded steady-state amplitude. This resonance phenomenon, which has no counterpart for plane collisions, was examined by analysing the transient development of the secondary beams triggered by a resonant collision. The transient response at resonant conditions is a slowly varying beam-like disturbance with modulated profile and amplitude that grows in time like $t^{1/2}$. Similarly to the forced response at a cut-off frequency, this continuously growing beam amplitude at resonance is caused by the accumulation of energy in the vicinity of the wave source, which here coincides with the interaction region of the colliding beams. As a result,

nonlinear as well as viscous effects are expected to play an important part in the transient evolution of the response near resonance. An asymptotic theory taking these effects into account, as well as fully numerical and experimental investigations of resonant collisions, would be highly desirable.

As noted in § 1, oblique collisions of wave beams could arise in the field from the interaction of the tide with three-dimensional bottom topography. In this context, the Earth's rotation, which is a significant factor in tidal-conversion processes, may influence the generation of secondary beams due to collisions of tidally induced beams. The present theory can be readily extended to account for the effects of background rotation. Briefly, for gravity–inertia waves owing to the combined action of buoyancy and Coriolis effects, the dispersion relation (2.6) is replaced by

$$\omega^2 = \sin^2\theta + f^2\cos^2\theta, \tag{8.1}$$

f being the ratio of the Coriolis parameter to the Brunt–Väisälä frequency (under typical conditions in the ocean, $f \leqslant 0.1$). Accordingly, a plane wave beam of frequency ω ($f < \omega < 1$) now propagates at a smaller angle θ to the horizontal,

$$\sin\theta = \frac{\sqrt{\omega^2 - f^2}}{\sqrt{1 - f^2}}. \tag{8.2}$$

With this modification, the kinematic analysis of § 3 can be repeated along similar lines, leading to equations analogous to (3.13), (3.14), (3.25) and (3.26) for the obliqueness of radiated secondary beams. Details, including a discussion of the effect of rotation on resonant collisions, will be reported elsewhere.

Acknowledgements

The authors wish to thank Professor T. Kataoka for enlightening discussions on the physical interpretation of resonant beam collisions. This work was supported in part by the National Science Foundation under grants DMS-098122 and DMS-1107335.

Appendix. Forcing terms of secondary beams

By substituting the primary-beam profiles (4.3)–(4.6) into the forcing terms (4.18), after some algebra, we find the following expressions for the functions $Q_n^{\pm}$ and $S_n^{\pm}$ ($n = 1, \ldots, 4$) in (4.18):

$$Q_n^+(k_1) = \mathbb{C}_n^+ k_1^{n-1} A_1(k_1), \quad S_n^+(k_2) = k_2^{4-n} A_2(k_2) \quad (n = 1, \ldots, 4), \tag{A 1}$$

where

$$\mathbb{C}_1^+ = a_1(\sin\theta_1 + 2\sin\theta_2), \tag{A 2a}$$

$$\mathbb{C}_2^+ = \mp\cos\theta_2\omega^+(a_2 - a_1\cos\theta_1) + 2\left(\omega^+ + \frac{1}{\omega_2}\right) a_1 \sin\theta_1 \sin\theta_2 \cos\phi \pm \left(\omega^+ + \frac{1}{\omega_1}\right) a_3 \sin^2\theta_2, \tag{A 2b}$$

$$\mathbb{C}_3^+ = -\cos\theta_1\omega^+(a_2 - a_3\cos\theta_2) \pm 2\left(\omega^+ + \frac{1}{\omega_1}\right) a_3 \sin\theta_1 \sin\theta_2 \cos\phi + \left(\omega^+ + \frac{1}{\omega_2}\right) a_1 \sin^2\theta_1, \tag{A 2c}$$

$$\mathbb{C}_4^+ = \pm a_3(\sin\theta_2 + 2\sin\theta_1), \tag{A 2d}$$

with

$$a_1 = -\cot\theta_1 \sin\theta_2 \cos\phi \pm \cos\theta_2, \tag{A 3a}$$

$$a_2 = \pm 2\cos\theta_1 \cos\theta_2 \cos^2\phi - \cot\theta_2 \cos\theta_2 \sin\theta_1 \cos\phi - \cot\theta_1 \cos\theta_1 \sin\theta_2 \cos\phi, \tag{A 3b}$$

$$a_3 = -\cot\theta_2 \sin\theta_1 \cos\phi \pm \cos\theta_1. \tag{A 3c}$$

Also,

$$Q_n^-(k_1) = (-1)^n \mathbb{C}_n^- k_1^{n-1} A_1(k_1), \quad S_n^- = k_2^{4-n} A_2^*(k_2) \quad (n = 1, \ldots, 4), \tag{A 4}$$

where

$$\mathbb{C}_1^- = a_1(\sin\theta_1 - 2\sin\theta_2), \tag{A 5a}$$

$$\mathbb{C}_2^- = \mp\cos\theta_2 \omega^-(a_2 - a_1\cos\theta_1) + 2\left(\omega^- - \frac{1}{\omega_2}\right) a_1 \sin\theta_1 \sin\theta_2 \cos\phi \pm \left(\omega^- + \frac{1}{\omega_1}\right) a_3 \sin^2\theta_2, \tag{A 5b}$$

$$\mathbb{C}_3^- = -\cos\theta_1 \omega^-(a_2 - a_3\cos\theta_2) \pm 2\left(\omega^- + \frac{1}{\omega_1}\right) a_3 \sin\theta_1 \sin\theta_2 \cos\phi + \left(\omega^- - \frac{1}{\omega_2}\right) a_1 \sin^2\theta_1, \tag{A 5c}$$

$$\mathbb{C}_4^- = \pm a_3(2\sin\theta_1 - \sin\theta_2). \tag{A 5d}$$

In (A 2), (A 3) and (A 5), the upper (lower) sign holds when the colliding beam of frequency ω_2 propagates downwards (upwards) in z.

REFERENCES

AKYLAS, T. R. 1984 On the excitation of nonlinear water waves by a moving pressure distribution oscillating at resonant frequency. *Phys. Fluids* **27**, 2803–2807.

ARANHA, J. A., YUE, D. K. P. & MEI, C. C. 1982 Nonlinear waves near a cut-off frequency in an acoustic duct: a numerical study. *J. Fluid Mech.* **121**, 465–478.

BELL, T. H. 1975 Lee waves in stratified flows with simple harmonic time dependence. *J. Fluid Mech.* **67**, 705–722.

GERKEMA, T., STAQUET, C. & BOURUET-AUBERTOT, P. 2006 Decay of semi-diurnal internal-tide beams due to subharmonic resonance. *Geophys. Res. Lett.* **33**, L08604.

JIANG, C.-H. & MARCUS, P. S. 2009 Selection rules for the nonlinear interaction of internal gravity waves. *Phys. Rev. Lett.* **102**, 124502.

KHATIWALA, S. 2003 Generation of internal tides in an ocean of finite depth: analytical and numerical calculations. *Deep-Sea Res.* **50**, 3–21.

KING, B., ZHANG, H. P. & SWINNEY, H. L. 2010 Tidal flow over three-dimensional topography generates out-of-forcing-plane harmonics. *Geophys. Res. Lett.* **37**, L14606.

LAMB, K. G. 2004 Nonlinear interaction among internal wave beams generated by tidal flow over supercritical topography. *Geophys. Res. Lett.* **31**, L09313.

LIGHTHILL, M. J. 1978 *Waves in Fluids*. Cambridge University Press.

MCEWAN, A. D. 1973 Interactions between internal gravity waves and their traumatic effect on a continuous stratification. *Boundary-Layer Meteorol.* **5**, 159–175.

MOWBRAY, D. E. & RARITY, B. S. 1967 A theoretical and experimental investigation of the phase configuration of internal waves of small amplitude in a density stratified fluid. *J. Fluid Mech.* **28**, 1–16.

PEACOCK, T. & TABAEI, A. 2005 Visualization of nonlinear effects in reflecting internal wave beams. *Phys. Fluids* **17**, 061702.

STASHCHUK, N. & VLASENKO, V. 2005 Topographic generation of internal waves by nonlinear superposition of tidal harmonics. *Deep-Sea Res.* **I50**, 605–620.

TABAEI, A. & AKYLAS, T. R. 2003 Nonlinear internal gravity wave beams. *J. Fluid Mech.* **482**, 141–161.

TABAEI, A., AKYLAS, T. R. & LAMB, K. G. 2005 Nonlinear effects in reflecting and colliding internal wave beams. *J. Fluid Mech.* **526**, 217–243.

ZHANG, H. P., KING, B. & SWINNEY, H. L. 2007 Experimental study of internal gravity waves generated by supercritical topography. *Phys. Fluids* **19**, 096602.